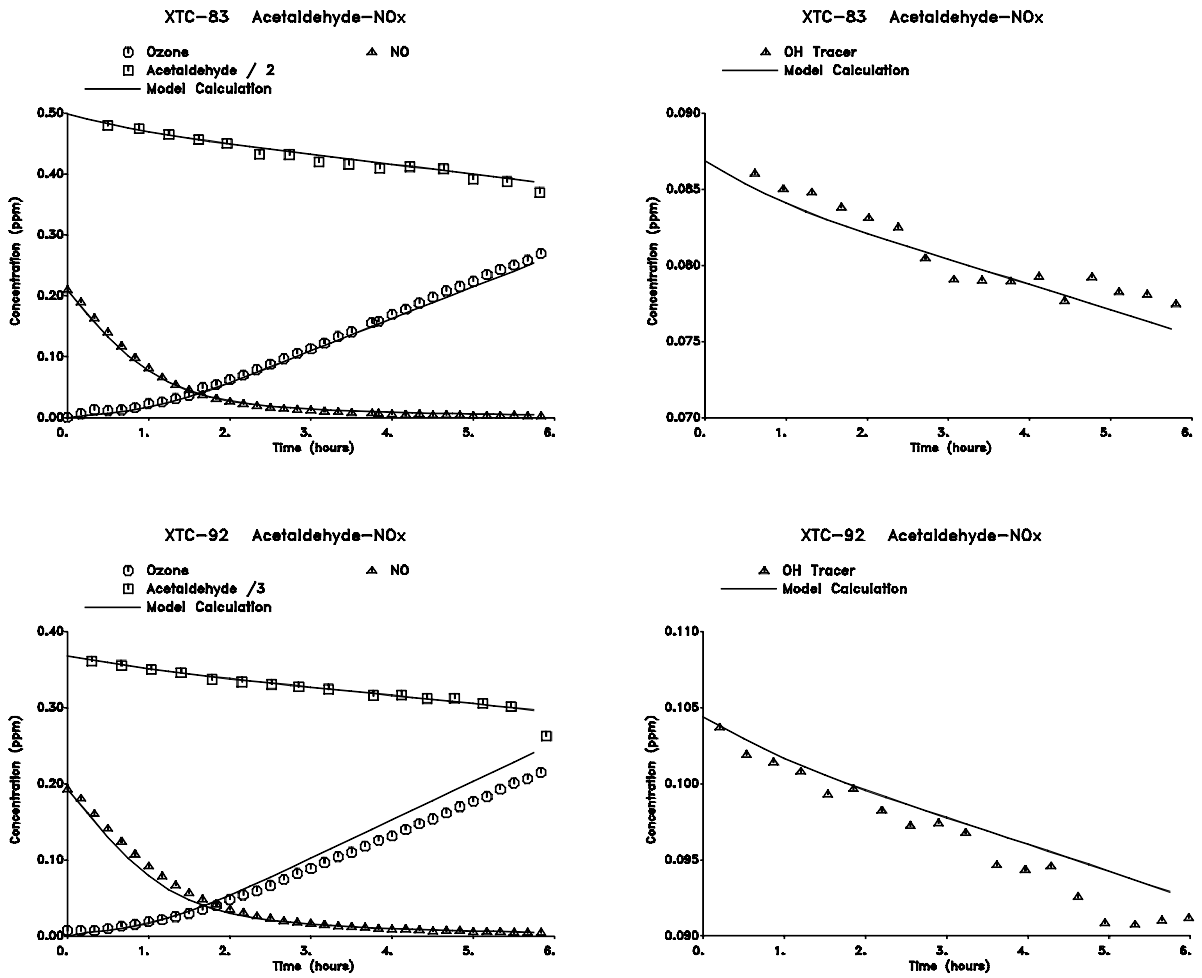

Figure 12. Experimental and calculated concentration-time profiles for selected species in the acetaldehyde - NO_x runs carried out in the xenon arc chamber.

and on Figure 16 for those using the ethane surrogate. Incremental reactivity plots are given on Figure 17. Results of model simulations are also shown. Note that all of these are summer runs carried out under clear sky conditions.

Figures 15 and 16 shows that the model consistently underpredicts the ozone formation rates in the base case experiments. This underprediction may be due to the relatively high temperatures for these runs, and the fact that the mechanisms for most species have not been evaluated at these higher temperatures. The relatively good performance in the case of the acetaldehyde runs may be due to the fact that the temperature dependencies for its main temperature-dependent reaction — the decomposition of PAN — are now reasonably well characterized. One might have expected better performance in the case of

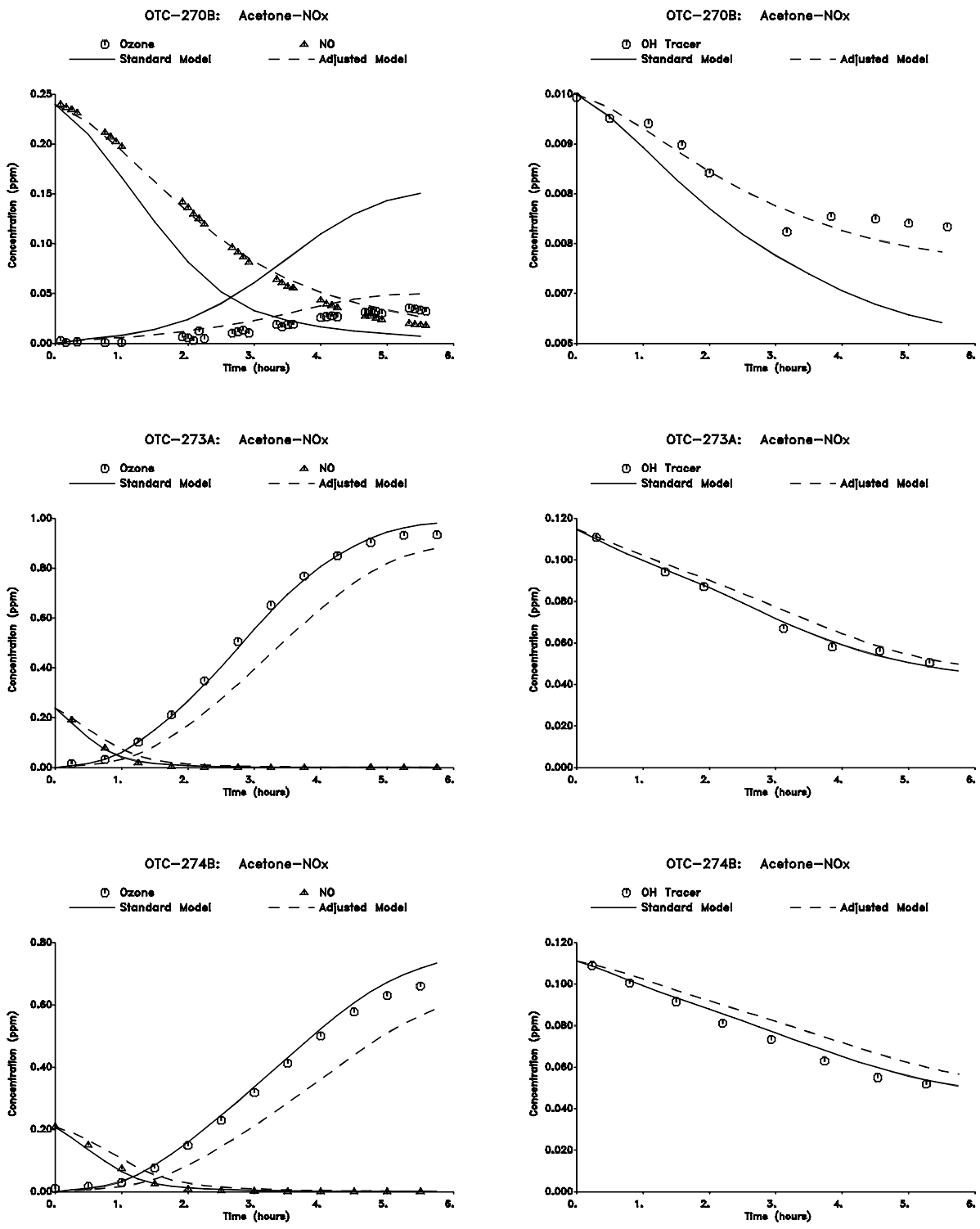

Figure 13. Experimental and calculated concentration-time profiles for selected species in the acetone - NO_x runs carried out in the outdoor chamber.

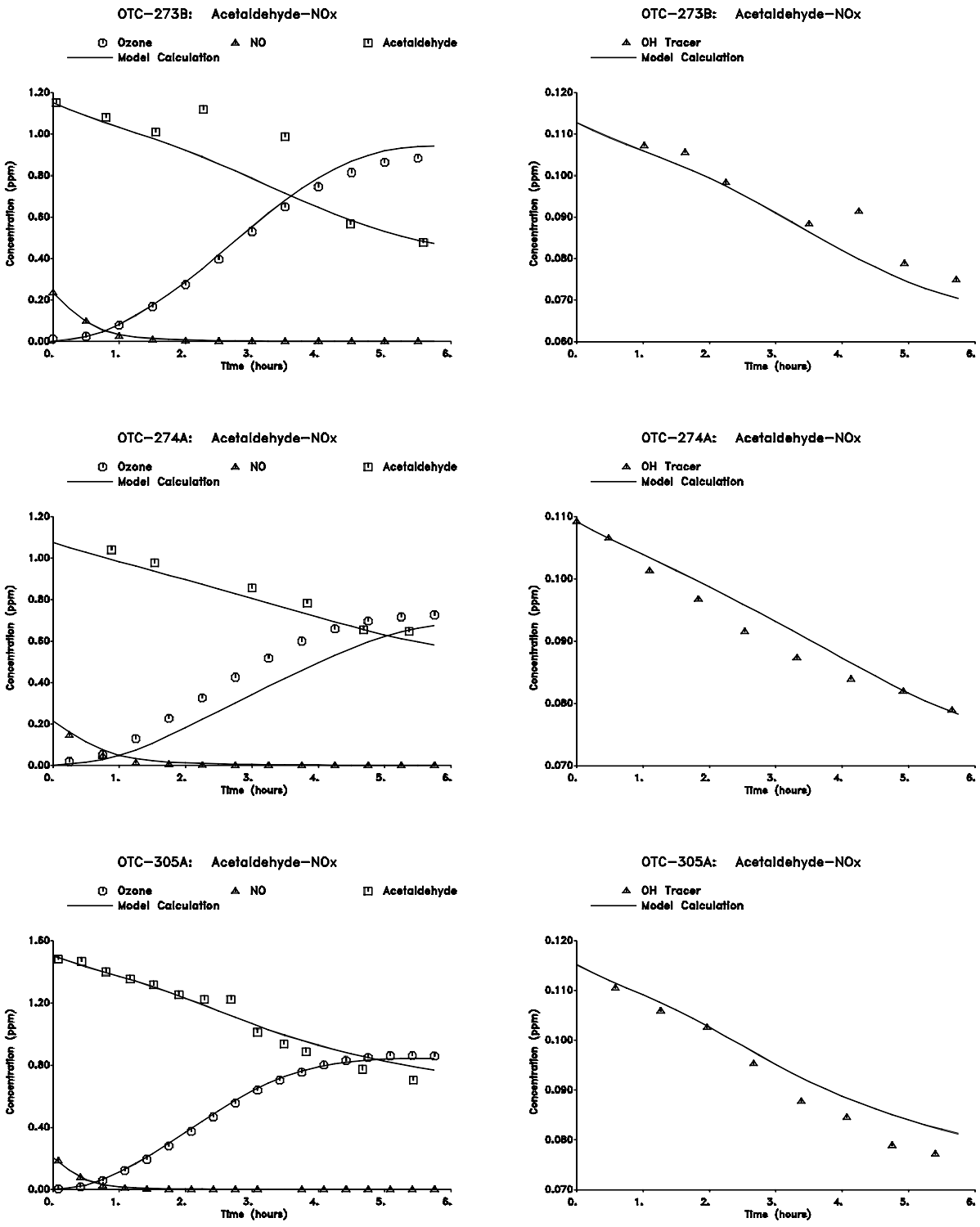

Figure 14. Experimental and calculated concentration-time profiles for selected species in the acetaldehyde - NO_x runs carried out in the outdoor chamber.

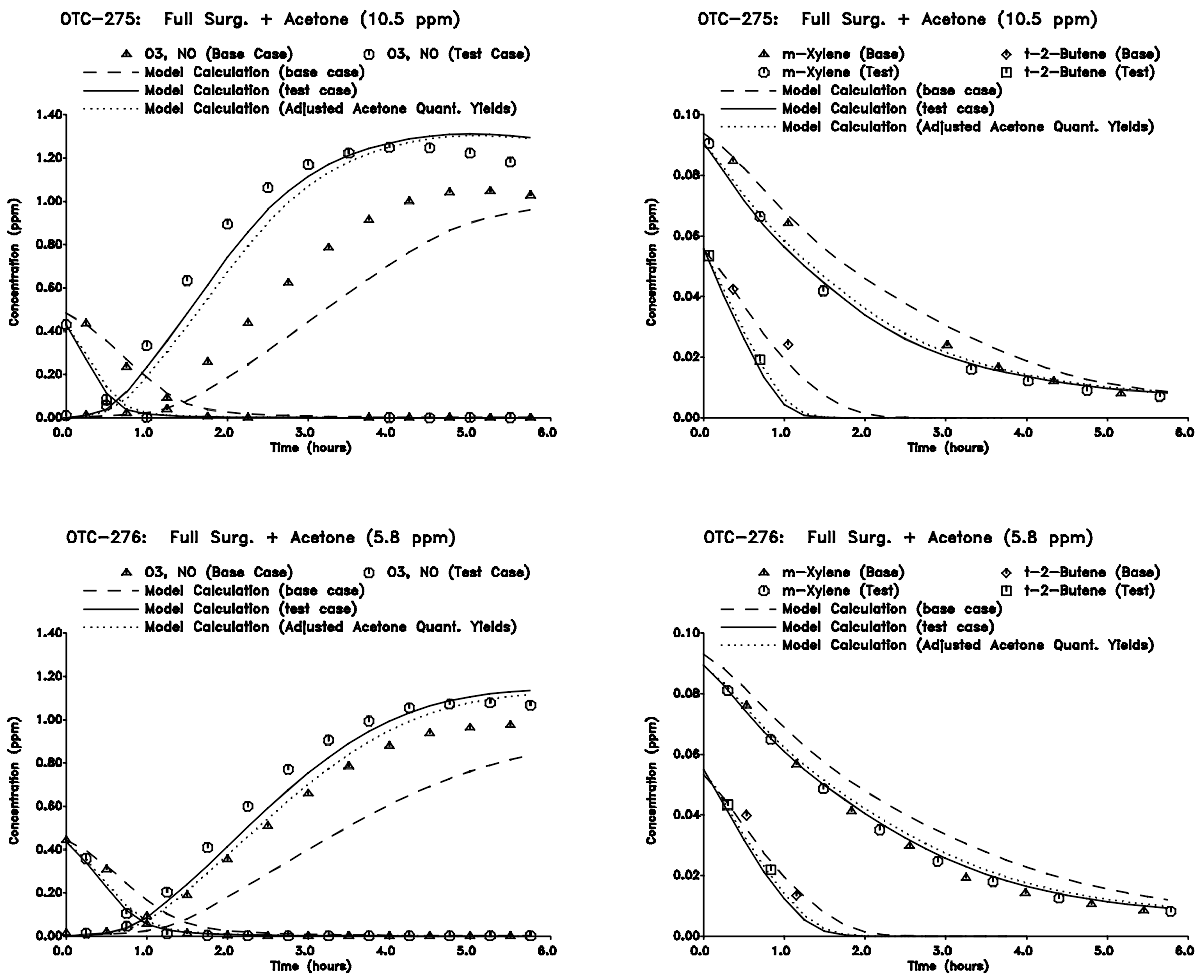

Figure 15. Experimental and calculated concentration-time profiles for selected species in a in the added acetone reactivity experiments using the full surrogate in the outdoor chamber.

the ethene runs, but the temperature dependence of the radical yields in the O_3 + ethene reaction have not been characterized, and adjustment of this radical yield can significantly improve the results of the model simulations of these runs. However, an investigation of the reasons for the discrepancies in the model simulations of the ethene and full surrogate runs is beyond the scope of this program.

Figure 17 shows that the model does not simulate the reactivity results very well, especially in the later periods of the runs. The biases of the model predictions later in the runs are also not consistent from run to run — in some cases the reactivities are reactivities are overpredicted, and in some cases they are underpredicted. This can be attributed, at least in part, to the poor performance of the model in simulating the base case experiments. The model gives somewhat better predictions of the incremental

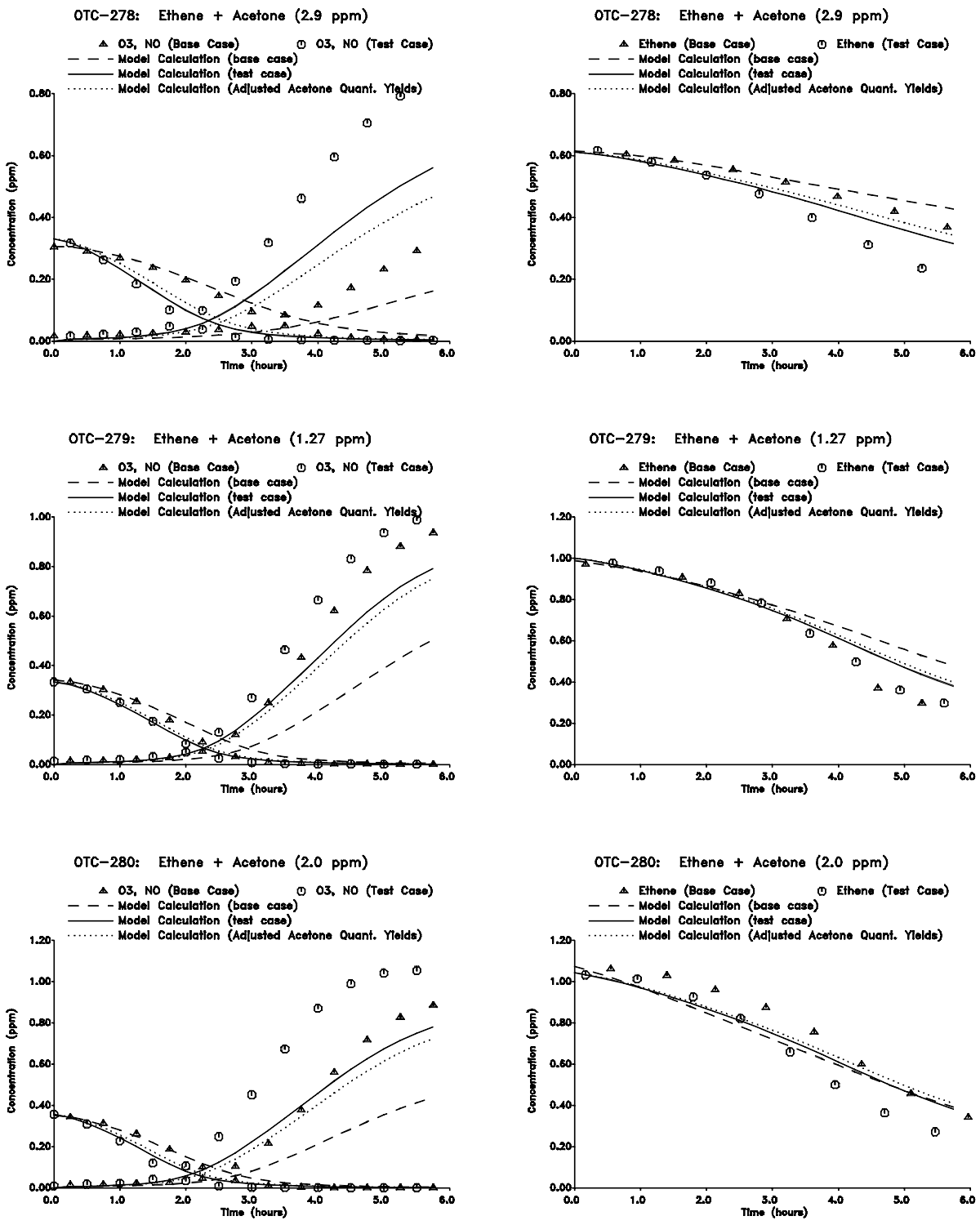

Figure 16. Experimental and calculated concentration-time profiles for selected species in a in the added acetone reactivity experiments using the ethene surrogate in the outdoor chamber.

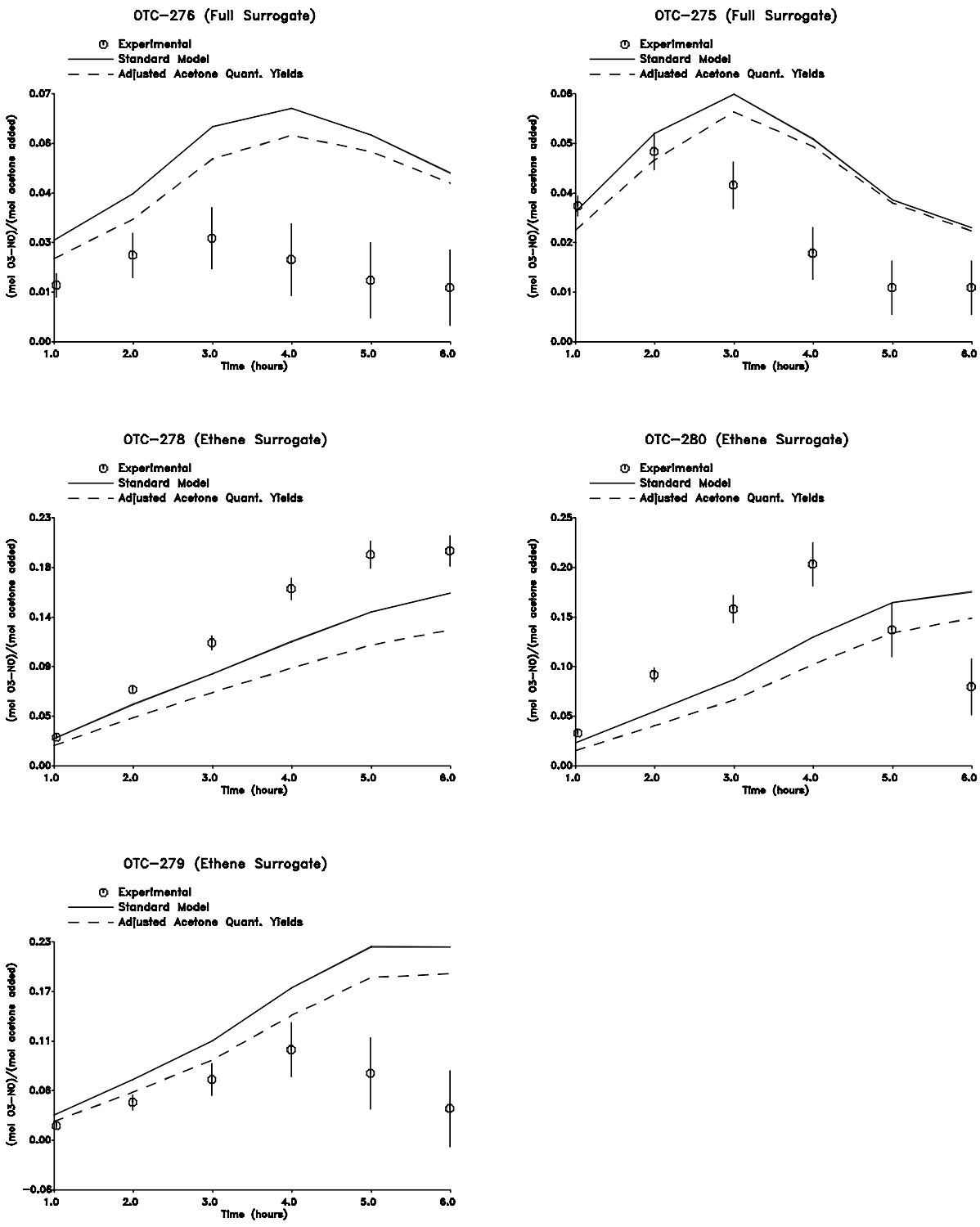

Figure 17. Experimental and calculated incremental reactivities, as a function of reaction time, in the added acetone reactivity experiments carried out in the outdoor chamber.

reactivities at earlier periods in the runs, before the predictions of the model for the base case experiment began to deviate significantly from the data. However, until the problems which caused the poor performance of the model in simulating the base case runs are addressed, we consider the outdoor chamber acetone reactivity experiments to be inconclusive and not useful for mechanism evaluation.

Ethane vs Acetone Comparison Experiments

Two outdoor chamber experiments were conducted on the outdoor chamber where the effects of adding approximately equal masses of acetone or ethane to a full surrogate - NO_x mixture were determined. In the first experiment (run OTC-312), the acetone was added to Side A (on the eastern side) while ethane was added to side B, while in the second experiment (OTC-313) the sides were reversed. For control purposes, a side equivalency test, where equal amounts of the surrogate - NO_x mixture were irradiated on both sides without any other additions, was also carried out. The same amount of surrogate and NO_x was used in all three runs. The conditions and selected results of these experiments are shown on Table 2, and selected results are shown on Figure 18. Note that the temperature was much higher in run OTC-312 than in the other two runs, and as a result much more ozone was formed than in run OTC-313, despite the fact that essentially the same reactant concentrations were employed.

The results of both acetone vs ethane experiments suggest that acetone has a slightly greater ozone reactivity than ethane under the conditions of these experiments. However, the differences are not the same in the two runs. In the higher temperature run (OTC-312), the NO oxidation and ozone formation rates were somewhat faster on the acetone side compared to the ethane side, though the final ozone yields were essentially the same. On the other hand, in the lower temperature run (OTC-313), the ozone formation and NO oxidation rates were essentially equal on both sides until the last hour, when slightly more ozone was formed on the side with acetone. The side equivalency test showed that the NO oxidation and ozone formation rate is slightly faster on the eastern side (Side A), presumably due to the fact the sun is to the east in the mornings. However, the effect of the side differences is small compared to the differences observed in run OTC-312. Since acetone is on the less reactive side in run OTC-313, where the acetone and ethane sides had equal NO and ozone results for most of the run, this suggests that the NO oxidation and ozone formation rates might have been slightly higher on the acetone side had this inequivalency not existed. On the other hand, the apparent greater reactivity of acetone relative to ethane would have been reduced in run OTC-312, where acetone is on the more reactive side.

The results of model simulations of these experiments are also shown on Figure 18. As with the other OTC runs employing the full surrogate, the model consistently underpredicts the rate of ozone formation and NO oxidation. It also significantly overpredicts the differences in reactivity between acetone and ethane in the lower temperature run, and the differences in final ozone yields in the higher temperature run.

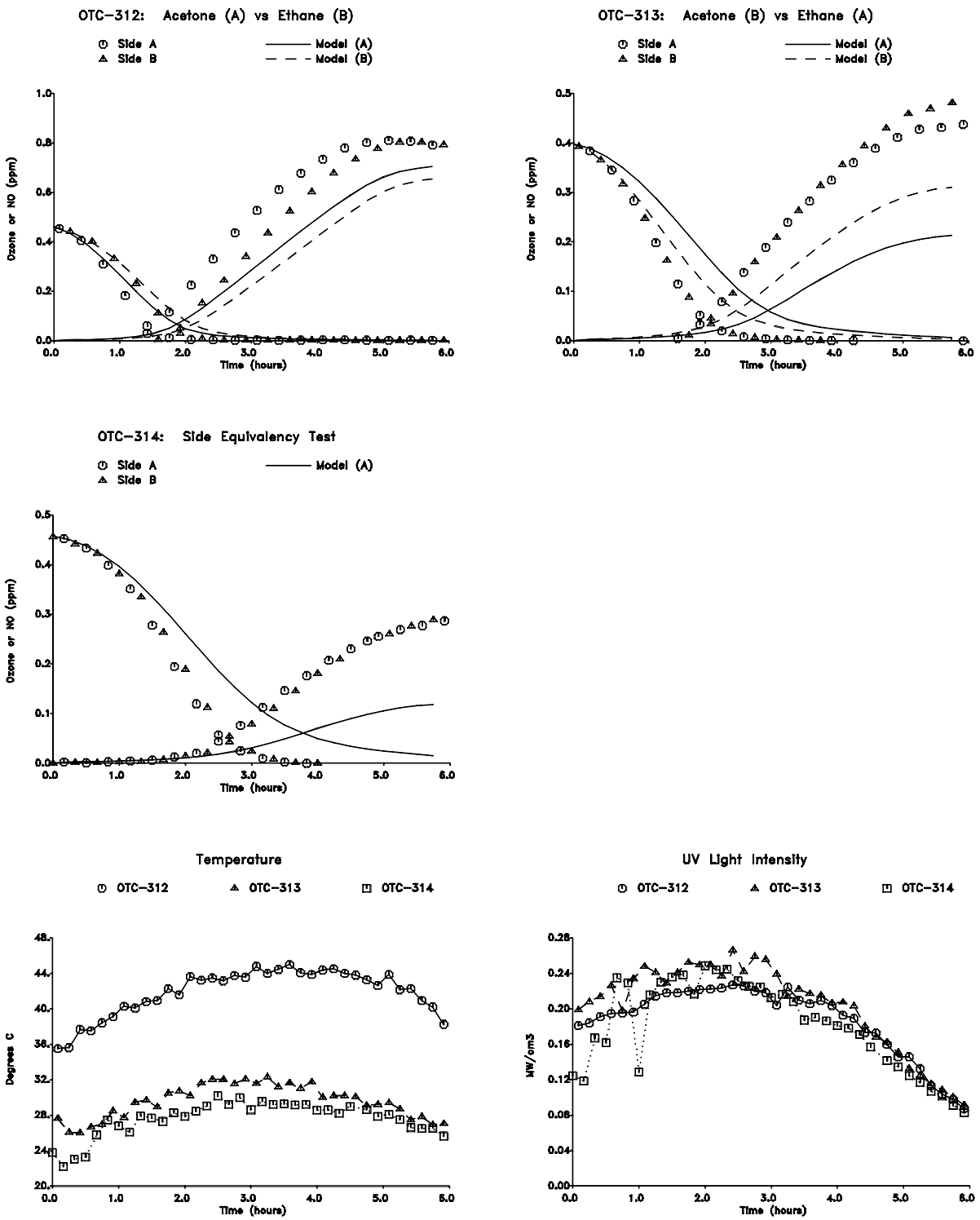

Figure 18. Experimental and calculated concentration-time profiles for ozone and NO, and experimental temperature and UV light intensity data, in the acetone vs ethane comparison experiments and the associated side equivalency test.

These results can be compared with the results of a very similar experiment reported by Jeffries (1993), where equal amounts of ethane and acetone (on a per carbon basis) were added to an ROG surrogate - NO_x mix on the two sides of the University of North Carolina (UNC) outdoor chamber, and simultaneously irriadiated. As with our OTC experiments, an equal amount of ethane was added on a per carbon basis as the ROG surrogate, but unlike our experiments the amount of acetone added had the same number of carbons, rather than the same mass, as the added ethane. This meant that the amount of acetone added was 28% higher, compared to added ethane, in the UNC experiment compared to our runs. Despite the relatively higher amount of added acetone, in the UNC experiment there was no measurable difference in the amount of ozone formed in the added acetone side compared to the added ethane side. Thus, either the reactivity difference was too small to be measured under the conditions of the UNC experiment, or acetone is slightly less reactive than ethane under the conditions of that run. This is in contrast with our results, where acetone was found to be very slightly more reactive in both experiments.

Although the runs (both ours and UNC's) need to be reproduced before definitive conclusions can be reached, the two OTC experiments suggest that the differences in reactivity of acetone and ethane may be temperature dependent, with the reactivities being nearly equal at the lower temperature (which is more representative of most ambient conditions), but with acetone becoming relatively more reactive as the temperature increases to above 40°C (104°F). A temperature effect in the differences of reactivity might be attributed to the relative importance of PAN formation in the photooxidation of acetone, since the decomposition of PAN to form radicals is highly temperature dependent. However, the average temperature in the UNC experiment was approximately 305°K, which is closer to (but slightly higher than) the lower temperature run in this study. Thus, a temperature effect cannot be the reason for the lower apparent reactivity of acetone relative to ethane in the UNC experiment compared to these runs. More research concerning effects of temperature on the base case system is needed before any conclusions can be made concerning the ability of the model to predict temperature effects on relative reactivities.

Model Simulations Using the Adjusted Acetone Mechanism

The model simulations of the acetone experiments in the chambers with the blacklight and xenon arc light sources, taken together, indicate that there is a problem with how the mechanism predicts the acetone photolysis rate is affected by the spectrum of the light source. Although the possibility of compensating errors can never be ruled out in model simulations of environmental chamber experiments (Jeffries et al., 1992), the fact that the model gives reasonably good fits to the results of the acetaldehyde experiments using the various light sources suggests that the discrepancies observed for acetone in these chambers are not likely to be due to errors in our characterization of experimental conditions. If the absorption cross sections are assumed to be correct (they are fairly straightforward to measure and there is no significant inconsistency in the literature concerning them) this discrepancy can only be explained by the model having an incorrect dependence of the quantum yields on wavelength. As discussed above, there are inconsistencies in the literature concerning the acetone quantum yields, and the accepted values

are based on analyses of chemical systems which are almost as complex as these chamber experiments.

The data in the literature do not provide any guidance for reducing the discrepancy, since the quantum yields we use in the model already are lower than any of the published values (see above). If we had not corrected the quantum yields of Meyrahn et al. (1986), or used the higher quantum yields of Gardner et al. (1984), the discrepancy between the model and our data from the blacklight chambers would be even worse. Therefore, the only option we have is to make arbitrary adjustments to the quantum yields to see if it is possible to make the model simulations more consistent with our experimental data.

We found that a factor of two downward adjustment of the photolysis rates resulted in a model which gave excellent predictions to the experimental incremental reactivities in the blacklight chamber, and somewhat better predictions of the results of the acetone - NO_x runs using that light source. This is shown on Figures 3-8, where the "adjusted acetone quantum yields" model uses acetone photolysis rates which are 54% of the value used in the standard model. However, if this adjustment is made by reducing the quantum yields by the same factor at all wavelengths, the result would be that the photolysis rate is also reduced by a factor of ~2 in the XTC runs, which would cause a significant underprediction of ozone formation in the acetone - NO_x runs in that chamber. This is shown in Figure 11, where the dotted lines show the model prediction where the acetone photolysis rate is reduced by approximately the same factor that gives the best fits to the blacklight chamber runs. Since the XTC light source has a spectrum which more closely resembles sunlight than do blacklights, this would clearly not be an acceptable adjustment for a model to be used in ambient simulations.

To fit both the blacklight and xenon arc chamber data, it is necessary to adjust the quantum yields such that the photolysis rates for the blacklight light source is reduced by ~2, while the rates with the xenon arc are relatively unchanged. A possible approach for doing this is suggested by examining the spectra of the light sources in the wavelength regions which affect acetone photolysis. Figure 1 shows the spectra of these light sources over the full wavelength region affecting most photolysis reactions, but shows that only a relatively narrow wavelength region, from ~290 - 320 nm, affects the photolysis of acetone. Figure 19 shows more clearly the spectra of the light sources, and the action spectrum for acetone, in the 300 - 320 nm wavelength region. It can be seen that the blacklights have a much lower intensity in this wavelength region than do the xenon lights or sunlight, which means that it would have a lower photolysis rate relative to that for NO_2. This should already be taken into account in the model simulations, since the spectra shown are used to calculate the photolysis rates. However, it also significant to note that the ratios of intensities of the xenon light to the blacklights increase significantly with increasing wavelength in this region. Therefore, the wavelength region affecting the acetone photolysis rates for blacklights is higher than that affecting the photolysis rate for the xenon arc light

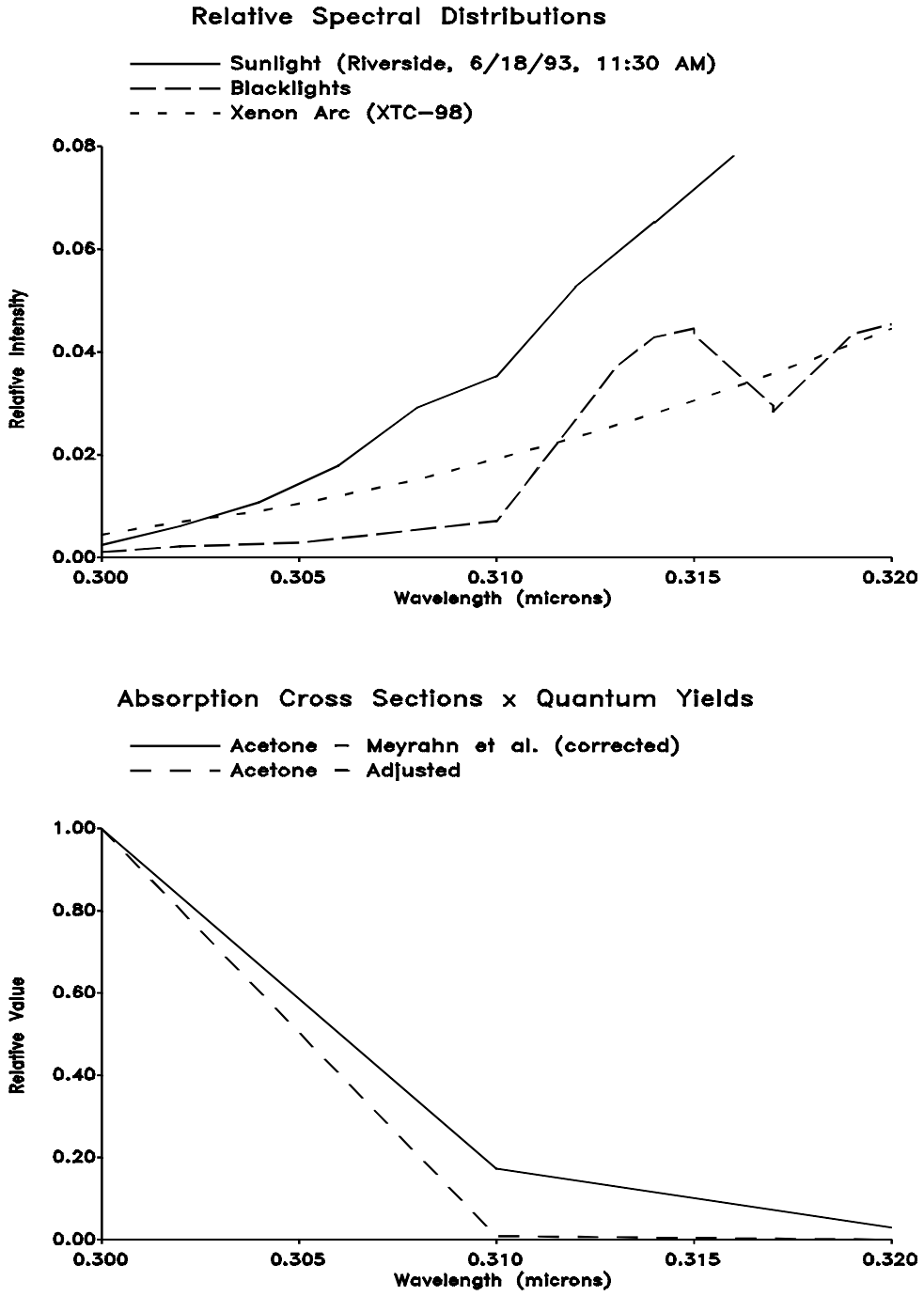

Figure 19. Top Plot shows comparison of spectra of light sources used in the environmental chamber studies, for the wavelength range 300 - 320 nm. Bottom plot shows spectra of absorption cross sections x quantum yields for the standard and the adjusted acetone mechanisms.

source. This means that decreasing the quantum yields at the higher wavelengths which are more important in affecting the rate in the blacklight chamber while increasing them at the lower wavelengths which are more important for the rate in the XTC might yield the desired photolysis rates under both conditions.

An adjusted acetone action spectrum which causes the desired reduction in the acetone photolysis rate with blacklights without significantly changing the photolysis rate in the XTC is shown on Figure 19. This spectrum results assuming that the quantum yield is essentially constant at ~0.6 at wavelengths below 290 nm, decreases to 0.005 at 310 nm, and to essentially 0 at 320 nm, in contrast with the corrected quantum yields of Meyrahn et al. (1986), where the quantum yields decrease more gradually with wavelength from ~0.6 at 290 nm to 0.01 at 320 nm and 0 at 330 nm. Thus the adjusted quantum yields are essentially the same as to those of Meyrahn et al (1986) at wavelengths ≤ 280 nm, are respectively ~2 and ~1.5 times higher at 290 and 300 nm, and are significantly lower at wavelengths ≥ 310 nm. (The specific quantum yields are given with the mechanism listing in Appendix A.) The model using this set of quantum yields is referred to as the "adjusted acetone" model. Although the set of quantum yields used in this adjusted model is not theoretically unreasonable, we have no justification for it other than its use results in significantly better fits to our chamber data.

The model simulations of our chamber experiments using the adjusted acetone model are shown on Figures 3-8 for blacklight chamber runs, on Figure 11 for the XTC runs, and on Figures 13 and 15-17 for the outdoor chamber runs. As discussed above, the improvement for the blacklight chamber runs is significant, though the adjusted model somewhat underpredicts the NO oxidation and ozone formation rates in run ETC-445 (Figure 3). On the other hand, the adjustment does not degrade the simulation of the acetone runs in the XTC (Figure 11); instead it slightly improves it. The adjusted model also gives a significantly better simulation of the wintertime outdoor acetone - NO_x run (OTC-270B), though the simulation of the summertime runs (OTC-273A and OTC-274B) are not quite as good as the unadjusted model (Figure 13). The changes in the predictions of the incremental reactivities in the outdoor runs (Figure 17) caused by the adjustment are relatively small compared to the discrepancy between the model calculation and the experimental data. Thus, the simulations of the outdoor runs are not sufficiently consistent to make any conclusions concerning which mechanism performs better. However, simulations of the better characterized indoor runs provide a much less ambiguous test of the mechanism, and the results indicate that the adjusted model performs significantly better in simulating acetone's reactivity and in predicting the effects of changing the spectrum of the light source.

ATMOSPHERIC REACTIVITY CALCULATIONS

Since incremmental reactivities of VOCs have been shown to be highly dependent on environmental conditions, incremental reactivities measured in environmental chamber experiments cannot necessarily be assumed to be applicable to atmospheric conditions (Carter and Atkinson, 1989). The only method available to obtain quantitative estimates of incremental reactivities of VOCs in ambient air pollution episodes is to conduct airshed model simulations of the episodes. Since these simulations cannot be any more reliable than the chemical mechanisms used, a major objective of this program was to assess the reliability of the acetone mechanism for use in such simulations. This was discussed in the previous sections. In this section, we discuss the results of model simulations of acetone's incremental reactivity in a variety of model scenarios representing ozone exceedence episodes in various areas in the United States (Bauges, 1990), and compare the results to incremental reactivities calculated for ethane and for the base ROG, i.e., the mixture representing total ROG emissions from all sources. Both the adjusted and the unadjusted acetone mechanism are used.

Scenarios Used for Reactivity Assessment

The set of airshed scenarios employed to assess acetone's reactivity for this study is the same as those used for calculating the MIR and other reactivity scales, as discussed previously (Carter, 1993a). The objective is to use a set of scenarios which represents, as much as possible, a comprehensive distribution of the environmental conditions where unacceptable levels of ozone is formed. Although a set of scenarios has not been developed for the specific purpose of VOC reactivity assessment, the EPA developed an extensive set of scenarios for conducting analyses of effects of ROG and NO_x controls on ozone formation using the EKMA modeling approach (Gipson et al., 1981; Gipson and Freas, 1983; EPA, 1984; Gery et al., 1987; Bauges, 1990). The EKMA approach involves use of single-cell box models to simulate how ozone formation in one day episodes is affected by changes in ROG and NO_x inputs. Although single-cell models cannot represent realistic pollution episodes in great detail, they can represent dynamic injection of pollutants, time-varying changes of inversion heights with entrainment of pollutants from aloft as the inversion height increases throughout the day, and time-varying photolysis rates, temperatures, and humidities (Gipson and Freas, 1981; EPA, 1984; Gipson, 1984; Hogo et al., 1988). Thus, they can be used to simulate a wide range of the chemical conditions which affect ozone formation from ROG and NO_x. These are the same as those affecting VOC reactivity. Therefore, at least to the extent they are suitable for their intended purpose, an appropriate set of EKMA scenarios should also be suitable for assessing methods to develop reactivity scales encompassing a wide range of conditions.

Base Case Scenarios

The set of EKMA scenarios used in this study were developed by the United States EPA for assessing how various ROG and NO_x control strategies would affect ozone nonattainment in various areas of the country (Bauges, 1990). The characteristics of these scenarios and the methods used to derive their input data are described in more detail elsewhere (Bauges, 1990; Carter, 1993a). Briefly, 39 urban areas in the United States were selected based on geographical representativeness of ozone nonattainment areas and data availability, and a representative high ozone episode was selected for each. The initial NMOC and NO_x concentrations, the aloft O_3 concentrations, and the mixing height inputs were based on measurement data for the various areas, the hourly emissions in the scenarios were obtained from the National Acid Precipitation Assessment Program emissions inventory (Bauges, 1990), and biogenic emissions were also included. Table 3 gives a summary of the urban areas represented and other selected characteristics of the scenarios.

Several changes to the scenario inputs were made based on discussions with the California ARB staff and others (Carter, 1993a). Two percent of the initial NO_x and 0.1% of the emitted NO_x in all the scenarios was assumed to be in the form of HONO. The photolysis rates were calculated using solar light intensities and spectra calculated by Jeffries (1991b) for 640 meters, the approximate mid-point of the mixed layer during daylight hours. The composition of the NMOCs entrained from aloft was based on the analysis of Jeffries et al (1989a). The composition of the initial and emitted reactive organics was derived as discussed below. Complete listings of the input data for the scenarios are given elsewhere (Carter, 1993a).

This set of 39 EKMA scenarios are referred to as "base case" to distinguish them from the scenarios derived from them by adjusting NO_x inputs to yield standard conditions of NO_x availability as discussed below. No claim is made as to the accuracy of these scenarios in representing any real episode, but they are a result of an effort to represent, as accurately as possible given the available data and the limitations of the formulation of the EKMA model, the range of conditions occurring in urban areas throughout the United States. When developing general reactivity scales it is more important that the scenarios employed represent a realistic distribution of chemical conditions than any accurately representing the details of any one particular episode.

The Base ROG mixture is the mixture of reactive organic gases used to represent the chemical composition of the initial and emitted anthropogenic reactive organic gases from all sources in the scenarios. Consistent with the approach used in the original EPA scenarios, the same mixture was used for all scenarios. The speciation for this mixture was derived by Croes (1991) based on an analysis of the EPA database (Jeffries et al. 1989a) for the hydrocarbons and the 1987 Southern California Air Quality Study (SCAQS) database for the oxygenates (Croes et al., 1993; Lurmann et al., 1992). This mixture consists of 52% (by carbon) alkanes, 15% alkenes, 27% aromatics, 1% formaldehyde, 2% higher

Table 3. Summary of conditions of base case scenarios used for atmospheric reactivity assessment.

City, State	Calc. Max O_3 (ppb)	ROG /NO_x	NO_x /NO_x^{MOR}	Final Height (km)	Init.+Emit Base ROG (mmol m^{-2})	Aloft O_3 (ppb)
Atlanta, GA	174	7.3	0.7	2.1	12	63
Austin, TX	171	9.3	0.5	2.1	11	85
Baltimore, MD	304	5.2	1.1	1.2	17	84
Baton Rouge, LA	235	6.8	1.0	1.0	11	62
Birmingham, AL	233	6.9	0.6	1.8	13	81
Boston, MA	191	6.5	0.6	2.6	14	105
Charlotte, NC	142	7.8	0.3	3.0	7	92
Chicago, IL	273	11.6	0.5	1.4	25	40
Cincinnati, OH	192	6.4	0.8	2.8	17	70
Cleveland, OH	239	6.6	1.0	1.7	16	89
Dallas, TX	192	4.7	1.3	2.3	18	75
Denver, CO	195	6.3	1.2	3.4	29	57
Detroit, MI	229	6.8	0.8	1.8	17	68
El Paso, TX	177	6.6	1.1	2.0	12	65
Hartford, CT	166	8.4	0.5	2.3	11	78
Houston, TX	291	6.1	1.0	1.7	25	65
Indianapolis, IN	201	6.6	0.9	1.7	12	52
Jacksonville, FL	152	7.6	0.7	1.5	8	40
Kansas City, MO	151	7.1	0.6	2.2	9	65
Lake Charles, LA	282	7.4	0.7	0.5	7	40
Los Angeles, CA	546	7.6	1.0	0.5	23	100
Louisville, KY	203	5.5	0.9	2.5	14	75
Memphis, TN	218	6.8	0.7	1.8	15	58
Miami, FL	131	9.6	0.4	2.7	9	57
Nashville, TN	163	8.1	0.5	1.6	7	50
New York, NY	350	8.1	0.8	1.5	39	103
Philadelphia, PA	230	6.2	1.0	1.8	19	53
Phoenix, AZ	258	7.6	1.0	3.3	40	60
Portland, OR	161	6.5	0.7	1.6	6	66
Richmond, VA	225	6.2	0.8	1.9	16	64
Sacramento, CA	194	6.6	0.9	1.1	7	60
St Louis, MO	301	6.1	1.1	1.6	26	82
Salt Lake City, UT	179	8.5	0.6	2.2	11	85
San Antonio, TX	126	3.9	1.1	2.3	6	60
San Diego, CA	186	7.1	1.0	0.9	8	90
San Francisco, CA	222	4.8	1.8	0.7	25	70
Tampa, FL	217	4.4	1.1	1.0	8	68
Tulsa, OK	216	5.3	0.9	1.8	15	70
Washington, DC	268	5.3	0.9	1.4	13	99

aldehydes, 1% ketones, and 2% acetylene. The detailed composition of this mixture is given elsewhere (Carter, 1993a).

Maximum Incremental Reactivity (MIR) and Maximum Ozone Reactivity (MOR) Scenarios

Incremental reactivities in the base case scenarios would be expected to vary widely, since incremental reactivities depend on the ROG/NO_x ratio, and that ratio varies widely among the base case scenarios. To obtain reactivity scales for specified NO_x conditions, a separate set of scenarios, designated MIR (for maximum incremental reactivity) and MOR (for maximum ozone reactivity) were developed (Carter, 1991, 1993a,b). In the MIR scenarios, the NO_x inputs were adjusted so the base ROG mixture (and most other VOCs) have their highest incremental reactivity. In the MOR scenarios, the NO_x inputs were adjusted to yield the highest ozone concentration. The changes in the base case ROG/NO_x ratios which yielded the MOR scenarios are given in Table 3. As discussed by Carter (1993a,b) the MIR ROG/NO_x ratios are ~1.4 times higher than MOR ratios in all cases.

NO_x Conditions in the Base Case Scenarios

As indicated above, the variability of ROG/NO_x ratios in the base case scenarios suggest a variability of reactivity characteristics in the base case scenarios. However, as discussed previously (Carter, 1993a,b), the ROG/NO_x ratio is also variable in the MIR or MOR scenarios, despite the fact that the NO_x inputs in these scenarios are adjusted to yield a specified reactivity characteristic. Thus, the ROG/NO_x ratio, by itself, is not necessarily a good predictor of reactivity characteristics of a particular scenario. The NO_x/NO_x^{MOR} ratio is a much better predictor of this, with values greater than 1 indicating relatively high NO_x conditions where ozone formation is more sensitive to VOCs, and values less than 1 indicating NO_x-limited conditions. NO_x/NO_x^{MOR} ratios less than 0.7 represent conditions where NO_x control is a more effective ozone control strategy than ROG control (Carter, 1993a,b). Note that more than half of the base case scenarios represent NO_x-limited conditions, and ~25% of them represent conditions where NO_x control is more beneficial than VOC control. A relatively small number of scenarios represent MIR or near MIR conditions. However, as discussed elsewhere (Carter, 1993a,b), this set of scenarios is based on near-worst-case conditions for ozone formation in each of the airsheds. Had scenarios representing less-than-worst-case conditions been included, one might expect a larger number of MIR or near MIR scenarios. This is because NO_x is consumed more slowly on days with lower light intensity or temperature, and thus the scenario is less likely to become NO_x-limited.

Incremental and Relative Reactivities

The incremental reactivity of a VOC in an airshed scenario is the change in ozone caused by adding the VOC to the emissions, divided by the amount of VOC added, calculated for sufficiently small amounts of added VOC that the incremental reactivity is independent of the amount added. The procedure used to calculate incremental reactivities in a scenario was as discussed in detail elsewhere (Carter, 1993a). The incremental reactivities depend on how the amount of VOC added are quantified. In this work, the

added VOC was quantified on a mass basis, since this is how VOCs are regulated. In addition, the incremental reactivities also depend on how ozone impacts are quantified (Carter, 1993a,b). In this work, two different ozone quantifications were used, resulting in two different incremental reactivities being calculated for a VOC in a scenario. These are discussed below.

The "Ozone Yield" incremental reactivities measure the effect of the VOC on the total amount of ozone formed in the scenario at the time of its maximum concentration. In this work, this is quantified as grams O_3 formed per gram VOC added. This gives the same ratios of incremental reactivities as reactivities calculated from peak ozone concentrations, but is preferred because it permits magnitudes of reactivities in scenarios with differing dilutions to be compared on the same basis. Most previous recent studies of incremental reactivity (Dodge, 1984; Carter and Atkinson, 1987, 1989, Chang and Rudy, 1990; Jeffries and Crouse, 1991) have all been based on ozone yield or peak ozone concentration reactivities.

The ozone yield incremental reactivities do not necessarily measure the effect of the VOC on exposure of unacceptable levels of ozone because it does not measure how long high levels of ozone is present. A quantification which reflects this is integrated ozone over the standard, which is defined as the sum of the hourly ozone concentrations for the hours when ozone exceeds the standard in the base case scenarios (Carter 1993a,b). In the previous work (Carter, 1993a,b), we used the California ozone standard of 90 ppb, but in this work we will use the national standard of 0.12 ppm. Reactivities relative to this quantification of ozone are referred to by the abbreviation "IntO_3>0.12" reactivities.

Relative reactivities are ratios of incremental reactivities to incremental reactivities of some standard VOC or mixture. Since these are the quantities which usually are the most relevant to control strategy applications, the results in this work will be given in terms of relative reactivities. In our previous work (Carter 1991, 1993a,b), we used the incremental reactivity of the base ROG mixture, i.e., the mixture representing ROG pollutants from all sources, as the standard to define relative reactivities. To be consistent with the terminology in the previous work, if the term "relative reactivity" is used without qualifier it refers to incremental reactivities relative to the base ROG mixture. However, because of the tendency within the EPA to consider ethane as the standard to define exempt vs controlled VOCs, we will also give reactivity ratios where ethane is used as the standard.

Reactivity Scales

A reactivity scale is a set of incremental or relative reactivities for a particular scenario or group of scenarios. Two types of reactivity scales will be discussed here, "base case" scales and adjusted NO_x scales. Base case scales are simply the set of incremental or relative reactivities in the 39 base case scenarios. Two sets of base case scales are derived — those based ozone yield reactivities and those based on IntO_3>0.12 reactivities. In the previous work (Carter, 1991, 1993a,b) we derived various multi-scenario scales from the individual base case scales by averaging or other procedures, to evaluate alternative

approaches for developing single reactivity scales for applications requiring single scales. However, the decision of whether to exempt a VOC should not be made based on relative reactivities of a single scale, but on a knowledge of the range of relative reactivities for a variety of conditions. Thus in this work we present the distribution of base case relative reactivities for the 39 individual scenarios rather than developing aggregated or optimum scales which represent the distribution by single numbers.

The adjusted NO_x incremental reactivity scales refer to the MIR (maximum incremental reactivity) or the MOIR (maximum ozone incremental reactivity) scales. These consist of averages of incremental reactivities MIR or MOIR scenarios, respectively. Relative reactivities in these scales are ratios of incremental reactivities in these scales. Reactivities in the MIR scale are of interest because the California Air Resources Board utilized an MIR scale to calculate reactivity adjustment factors in its clean fuels/low emissions vehicle regulations (CARB, 1991). The justification for using this scale in applications requiring a single scale (such as the CARB vehicle regulations) is that it reflects conditions where ozone is most sensitive to changes in VOC emissions, and complements NO_x control, which is most effective for reducing ozone under conditions where the MIR scale is least applicable (Carter, 1993a,b). The MOIR scale is preferred by many as an alternative for such applications because it reflects conditions which are most favorable for ozone, and is more representative of the distribution of conditions in the base case scenarios (Carter 1993a,b). Most other alternative reactivity scales which might be appropriate for assessing VOC control strategies (i.e., excluding scales representing highly NO_x-limited conditions where ozone is more sensitive to NO_x than VOCs) tend to fall in the range defined by the MIR and MOIR scales.

Note that the MIR, MOIR and base case scales derived in this work are somewhat different from those calculated previously (Carter, 1993a,b) because an updated chemical mechanism was used. Table 4 gives the MIR and MOIR incremental reactivities using the mechanism employed in this work and compares them with those calculated previously (Carter, 1993a,b), which were derived using the SAPRC-90 mechanism. The updates to the mechanism result in higher incremental reactivities for all species except for formaldehyde, acetone, and benzaldehyde, higher relative reactivities for internal alkenes, alkanes other than methane and benzene, lower relative reactivities for formaldehyde, acetone, and benzaldehyde, and slightly lower relative reactivities for most other species. The decrease in relative reactivity for formaldehyde and acetone, and increase for internal alkenes, are directly attributable to changes in their mechanisms as discussed above.

Calculated Relative Reactivities of Acetone and Ethane

Table 5 gives a tabulation of the relative reactivities of acetone and ethane in the various base case and MIR and MOIR reactivity scales calculated using the updated mechanism. Distribution plots of the relative reactivities of acetone and ethane in the base case scenarios are shown on Figure 20, Figures 21 gives distribution plots of the acetone/ethane incremental reactivity ratio for the base case scenarios, and

Table 4. Comparison of incremental and relative reactivities in the MIR and MOIR scales calculated using the updated and the SAPRC-90 mechanisms.

Compound	MIR Scale [a]				MOIR Scale [a]			
	SAPRC-90 IR	Updated IR	Change (%) IR	RR	SAPRC-90 IR	Updated IR	Change (%) IR	RR
CO	0.054	0.061	13%	-3%	0.038	0.040	4%	-10%
Methane	0.0150	0.016	10%	-6%	0.0093	0.0099	6%	-8%
Ethane	0.25	0.30	21%	4%	0.17	0.20	24%	6%
n-Butane	1.02	1.26	23%	5%	0.66	0.83	26%	9%
n-Octane	0.60	0.83	37%	17%	0.41	0.57	38%	19%
iso-Octane	0.93	1.16	25%	7%	0.54	0.72	33%	15%
n-Decane	0.46	0.68	46%	25%	0.31	0.47	51%	30%
Ethene	7.4	8.3	12%	-4%	3.2	3.4	6%	-9%
Propene	9.4	11.2	18%	1%	3.8	4.3	13%	-3%
trans-2-Butene	10.0	13.5	35%	16%	3.8	4.7	25%	7%
Isobutene	5.3	6.0	13%	-3%	1.9	2.0	4%	-10%
1-Hexene	4.4	5.7	30%	11%	1.7	2.3	31%	13%
Benzene	0.42	0.60	42%	22%	0.138	0.20	48%	27%
Toluene	2.7	3.2	16%	-1%	0.63	0.69	10%	-5%
m-Xylene	8.2	8.8	8%	-8%	2.5	2.5	2%	-12%
135-TM-Benzene	10.1	11.3	11%	-5%	3.1	3.2	4%	-11%
Methanol	0.56	0.63	11%	-5%	0.28	0.29	4%	-11%
Ethanol	1.34	1.6	21%	4%	0.72	0.90	24%	7%
Formaldehyde	7.2	7.0	-2%	-16%	2.1	1.9	-11%	-23%
Acetaldehyde	5.5	6.3	15%	-2%	2.2	2.4	12%	-3%
Acetone [b]	0.56	0.49	-13%	-25%	0.20	0.19	-7%	-20%
Benzaldehyde	-0.57	-0.24	58%	64%	-1.24	-1.41	-14%	2%
Cresols	2.3	2.6	13%	-3%	-0.58	-0.59	3%	-12%
Base ROG Mix	3.1	3.7	17%	0%	1.17	1.36	16%	0%

[a] IR = incremental reactivities in units of grams O_3 per gram VOC; RR = reactivity relative to base ROG mixture.
[b] Standard acetone mechanism.

Table 5. Relative ozone yield and $IntO_3$>0.12 reactivities and reactivity ratios for acetone and ethane in the base case scenarios and the MIR and MOIR scales.

Scenario or Scale	Base ROG IR [a]	Reactivities Relative to Base ROG — Ozone Yield Reactivities — Ethane	Acetone (Standard)	Acetone (Adjusted)	— IntO3 > 0.12 Reactivities — Ethane	Acetone (Standard)	Acetone (Adjusted)
Base Case Scenarios							
ATL GA	0.93	0.17	0.144	0.128	0.130	0.123	0.107
AUS TX	0.74	0.20	0.147	0.133	0.149	0.117	0.103
BAL MD	1.7	0.132	0.142	0.123	0.086	0.126	0.104
BAT LA	1.00	0.142	0.136	0.117	0.103	0.117	0.098
BIR AL	0.80	0.24	0.17	0.16	0.129	0.120	0.103
BOS MA	0.79	0.21	0.147	0.136	0.143	0.120	0.106
CHA NC	0.60	0.22	0.16	0.145	0.18	0.138	0.125
CHI IL	0.38	0.24	0.18	0.16	0.135	0.115	0.096
CIN OH	1.14	0.19	0.141	0.129	0.120	0.112	0.096
CLE OH	1.25	0.139	0.135	0.118	0.092	0.115	0.096
DAL TX	2.5	0.103	0.125	0.104	0.085	0.114	0.094
DEN CO	1.7	0.097	0.132	0.111	0.074	0.122	0.100
DET MI	1.02	0.20	0.144	0.130	0.121	0.114	0.098
ELP TX	1.5	0.104	0.130	0.107	0.081	0.118	0.095
HAR CT	0.86	0.21	0.15	0.140	0.16	0.130	0.116
HOU TX	1.21	0.17	0.140	0.125	0.104	0.111	0.094
IND IN	1.37	0.15	0.131	0.115	0.110	0.116	0.098
JAC FL	0.82	0.16	0.137	0.120	0.143	0.126	0.109
KAN MO	1.10	0.20	0.143	0.131	0.16	0.124	0.111
LAK LA	0.60	0.21	0.15	0.138	0.135	0.118	0.099
LOS CA	0.77	0.121	0.128	0.110	0.075	0.106	0.084
LOU KY	1.36	0.18	0.144	0.129	0.128	0.119	0.103
MEM TN	0.89	0.20	0.15	0.138	0.126	0.119	0.102
MIA FL	0.61	0.19	0.148	0.133	0.18	0.141	0.127
NAS TN	0.81	0.24	0.17	0.16	0.19	0.149	0.135
NEW NY	0.45	0.16	0.130	0.114	0.084	0.100	0.080
PHI PA	1.20	0.16	0.135	0.121	0.105	0.116	0.099
PHO AZ	1.41	0.144	0.139	0.121	0.093	0.115	0.095
POR OR	1.08	0.18	0.139	0.125	0.142	0.124	0.108
RIC VA	1.11	0.18	0.144	0.132	0.110	0.120	0.103
SAC CA	1.29	0.16	0.15	0.132	0.125	0.133	0.115
SAI MO	1.42	0.124	0.137	0.119	0.081	0.120	0.101
SAL UT	0.94	0.19	0.16	0.140	0.128	0.125	0.108
SAN TX	1.8	0.124	0.126	0.107	0.120	0.124	0.105
SDO CA	0.98	0.110	0.109	0.090	0.085	0.099	0.078
SFO CA	1.9	0.053	0.146	0.116	0.050	0.142	0.114
TAM FL	1.8	0.123	0.132	0.113	0.094	0.119	0.099
TUL OK	1.27	0.17	0.137	0.124	0.120	0.118	0.103
WAS DC	1.07	0.19	0.146	0.132	0.110	0.112	0.096
Average	1.13	0.166	0.142	0.126	0.118	0.120	0.103
Adjusted NO_x Scales							
MIR Scale	3.7	0.082	0.133	0.110			
MOIR Scale	1.36	0.150	0.139	0.121			

[a] Incremental reactivity in units of gm O3/gm VOC.

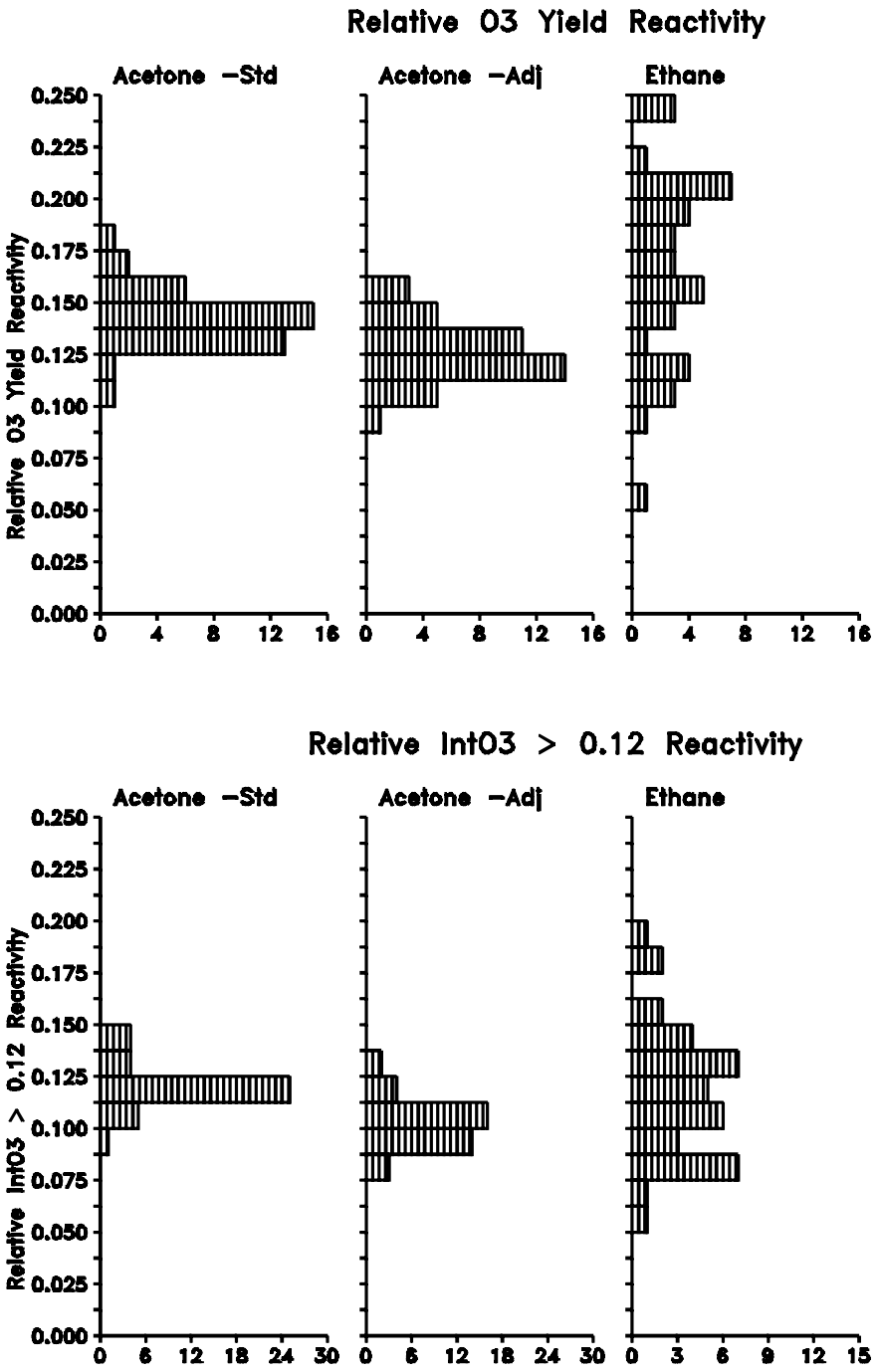

Figure 20. Distribution plots of ozone yield and $IntO_3$>0.12 reactivities, relative to the base ROG mixture, for acetone and ethane in the base case scenarios.

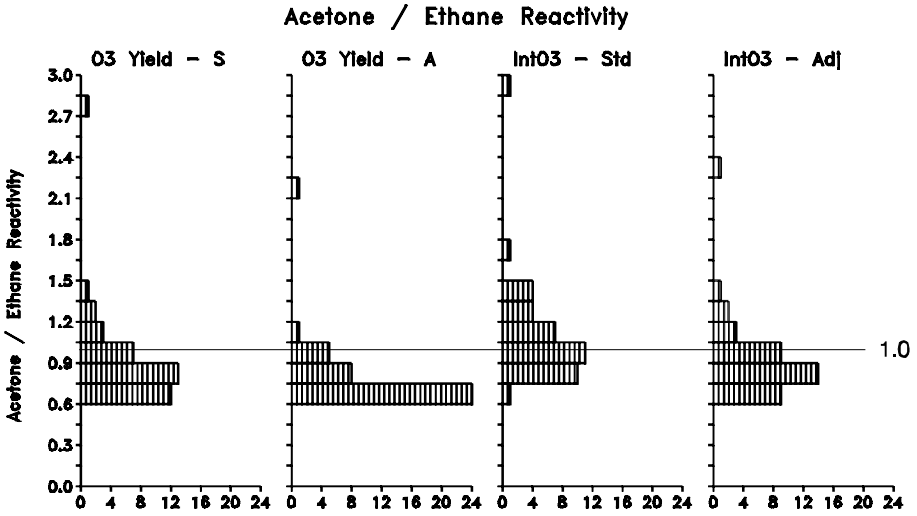

Figure 21. Distribution plots of ratios of ozone yield and $IntO_3$>0.12 reactivities of acetone relative to ethane for the base case scenarios.

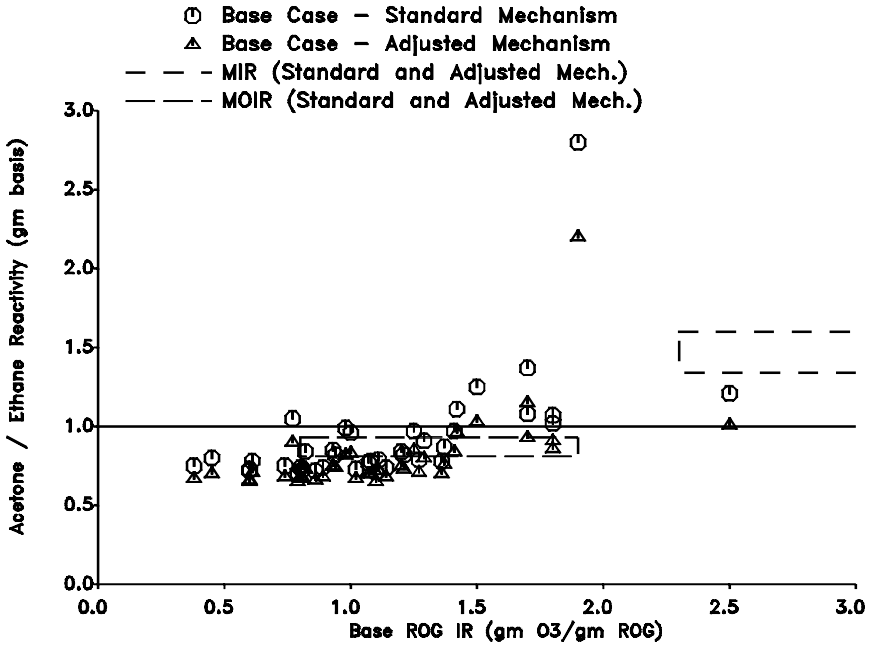

Figure 22. Plots of ratios of ozone yield reactivities of acetone relative to ethane against the incremental reactivity of the base ROG for the base case scenarios. Reactivity ratios and ranges of base ROG reactivities for the MIR and MOIR scales are also shown.

figure 22 plots the acetone/ethane reactivity ratios against the incremental reactivity of the base ROG. Reactivities of acetone were calculated both using the standard updated mechanism and using the mechanism with the acetone quantum yields adjusted to fit the blacklight and xenon arc chamber data as discussed above.

It can be seen that the adjustment to the acetone mechanism to fit the chamber data causes a slight (~13%) reduction in the incremental and relative reactivity of acetone. This is a fairly small difference compared to the variability of its relative reactivity or reactivity relative to ethane. The differences between these two calculations can be thought of as an indication of the lower limit to the chemical uncertainty in calculations of acetone's reactivity.

Figures 21 and 22 show that acetone is less reactive than ethane in a majority of the base case scenarios, though there are a few scenarios where acetone is slightly more reactive, and one where the unusually low relative reactivity of ethane results in an unusually high acetone/ethane reactivity ratio. The reactivity ratio in this case does not appear to be significantly affected by how O_3 is quantified — though it should be noted that this is not the case for all VOCs (Carter 1993a,b). Figure 22 shows that the reactivity ratio tends to increase as the reactivity ratio increases above the range which is characteristic of maximum ozone conditions. Thus, although acetone is of equal or lesser reactivity to ethane in most scenarios, its reactivity relative to ethane tends to increase as the scenario becomes more sensitive to VOC emissions. Because of this, incremental reactivity of acetone in the MIR scale is calculated to be 1.3 or 1.6 times higher than that of ethane, depending on whether the quantum yields are adjusted to fit the chamber data. However, all but one of the base case scenarios have lower reactivity ratios than in the MIR scale. The distribution of reactivity ratios in the base case scenarios is better represented by the reactivity ratio in the MOIR scale, where acetone is calculated to be slightly less reactive than ethane.

An alternative — and we believe more relevant — standard for assessing whether to regulate emissions of a compound is its reactivity relative to the mix of all other emitted VOCs, or the base ROG mixture. Figure 20 shows that the relative reactivities of acetone varies over a much narrower range than those for ethane, though the variation is somewhat less when ozone is quantified by integrated O_3 over the standard. The range of ozone yield relative reactivities are 0.05 - 0.24 for ethane and 0.11 - 0.18 for acetone with the more reactive standard mechanism. Thus acetone with the standard mechanism is between 5.6 - 9 times less reactive in terms of ozone yields than the base ROG, while ethane is between 4 - 20 times less reactive. For ozone yield reactivities, the ranges of relative reactivities are 0.074 - 0.19 for ethane and 0.10 - 0.15 for the standard acetone mechanism. Thus acetone with the standard mechanism is between 7 - 10 times less reactive in terms of integrated ozone over the standard than the base ROG, while ethane is 5 - 13 times less reactive. The MIR and MOIR relative reactivities are within these ranges.

It is interesting to note that the scenarios where acetone looks the most reactive compared to ethane are not necessarily the same as those where acetone has the highest reactivity relative to the base ROG mixture. From Figure 21 it can be seen that there is one scenario where the acetone/ethane reactivity ratio is unusually high, being 3 for the unadjusted mechanism. However, Table 5 shows that the corresponding ozone yield relative reactivity for the unadjusted acetone mechanism in that scenario is only 0.146, which is very close to the average for all scenarios. Thus the high acetone/ethane reactivity ratio in that case is due entirely to an unusually low relative reactivity for ethane. Furthermore, the scenario with the highest relative reactivity for acetone has an acetone/ethane reactivity ratio of ~0.75 for the standard mechanism, which is lower than average. In general, because the relative reactivity of ethane is so much more variable than that of acetone (as shown on Figure 20), it is the reactivity of ethane which is the primary factor which determines the reactivity of acetone relative to ethane.

CONCLUSIONS

The decision whether it is appropriate to regulate a compound as an ozone precursor requires a qualitative assessment of its reactivity relative to ozone formation under a variety of environmental conditions. This requires developing and experimentally validating a chemical mechanism for the compounds relevant atmospheric reactions, which can then be used in airshed models to predict its atmospheric reactivity. Although mechanisms for the atmospheric reactions of acetone have been available for some time, until this study there have been no reliable data available to evaluate their accuracy when used in such models. The major objective of this study was to provide the data needed for this purpose.

The data base which was developed to evaluate the mechanism of acetone is now more extensive than that for a vast majority of the other VOCs emitted into the atmosphere, including many which are far more important in contributing to the ozone problem. Acetone has been studied in NO_x-air environmental chamber irradiations by itself and in the presence of other reactive VOCs, and experiments utilizing a variety of light sources, including natural sunlight and artificial lights closely resembling natural sunlight. Although the incremental reactivity experiments in the outdoor chamber are inconclusive because of the inability of the model to simulate the base case conditions, the outdoor chamber experiments with acetone in the absence of other added VOCs, and the wide variety of indoor chamber experiments, provide a useful data base for evaluating acetone's mechanism. The indoor runs using the blacklights provide information concerning the effects of acetone on ozone formation under a wide variety of conditions, and the runs using the xenon arc light source provide information concerning acetone which more closely resembles sunlight. The difference in spectral distribution of the blacklight and xenon arc light sources provide a valuable means to test the model for how the photolysis of acetone depends on light spectrum. This is important because the spectrum of ambient sunlight is not constant, it varies significantly depending on the time of day, day of year, and the extent of atmospheric haze and the tropospheric ozone column.

An examination of the recent literature and reviews concerning the atmospheric reactions of acetone indicate that the mechanism we have previously used for acetone (Carter, 1990) needed to be updated in some respects. The greatest uncertainty in the acetone photooxidation mechanism is the quantum yields for its photolysis, concerning which the data in the literature are not in agreement. The evaluations (e.g., Atkinson et al., 1992) recommend the models use the data of Meyrahn et al. (1986), but our model simulations of their experiments indicate that the quantum yields in longest wavelengths (where sunlight and blacklights are more intense) are unreliable and need correction. The acetone mechanism used in our model was updated to be consistent with the latest evaluations in the literature, and to incorporate the estimated correction to the quantum yield data of Meyrahn et al (1986). These corrections

had a tendency to make acetone somewhat less reactive than was previously predicted, but still of comparable reactivity to ethane.

The updated mechanism was found to simulate reasonably well the results of the experiments using the indoor chamber light source most closely resembling sunlight and the outdoor chamber runs which were conducted during the summer. However, this mechanism consistently overpredicted the rate of ozone formation in the blacklight chamber experiments and also overpredicted the ozone formation in the wintertime acetone - NO_x run in the outdoor chamber. It is considered unlikely that this is due to incorrect characterization of the blacklight intensity or spectra, because the model could give good simulations of the photochemical reactivity of acetaldehyde, a VOC which photolyzes in a similar wavelength region as acetone. Thus it appears likely that the problem is that the model incorrectly represents how the acetone photolysis quantum yields depend on wavelength.

An adjusted version of the updated acetone mechanism was developed which was considerably more successful in simulating the data base developed in this study. The adjustment involves assuming that the quantum yields fall off with increasing wavelength much more rapidly than indicated by the data of Meyrahn et al. (1986), but that the fall off begins at a slightly longer wavelength. Although this adjustment is not theoretically unreasonable, there is no basis for it other than fitting these environmental chamber data, which are highly complex chemical systems with a number of other potential sources of error. The possibility that the problem may be due to an incorrect characterization of the effect of the mercury lines in the blacklight light source cannot be entirely ruled out. Therefore, in the assessment of the reactivities of acetone in the atmosphere, both the unadjusted (or standard) mechanism and the adjusted acetone mechanism were used in the model calculations. A comparison of the predictions of the two mechanisms give an indication of the approximate minimum magnitude of the effects of chemical mechanistic uncertainties associated with calculations of acetone's atmospheric reactivity.

It was found that the adjustment to the acetone quantum yields to fit our chamber data caused an approximately 13% reduction in the calculated incremental reactivity of acetone under atmospheric conditions. This is a relatively small effect compared to the extent to which the relative reactivity of acetone varied with atmospheric conditions. Thus it is concluded that although there are uncertainties in acetone's quantum yields, the effect of this uncertainty is not large enough to substantively affect conclusions concerning the range of acetone's effect on ozone production under conditions represented by the model scenarios we employed. However, the effect may be larger in model simulations of wintertime conditions, since the adjustment has the greatest effect under lighting conditions which have relatively low intensity in the UV. Since all the scenarios used in this study were based on worst case or near-worst case conditions, conditions of low UV intensity are not well represented.

The model simulations indicate that acetone is slightly less reactive than ethane in a majority of the scenarios representing worst-case or near-worst-case conditions. However, there was one scenario where the ethane was calculated to have an unusually low relative reactivity, resulting in acetone being calculated to be more reactive than ethane by factors of 2-3, depending on whether or not the adjusted quantum yields are used. In general, acetone becomes increasingly more reactive relative to ethane as NO_x conditions approach those yielding the highest incremental reactivities, with the result being that acetone has a slightly higher (by a factor of 1.3 to 1.6, depending on the quantum yields) MIR incremental reactivity than ethane. On the other hand, in the MOIR scale, which represents NO_x conditions most favorable for ozone formation, acetone is calculated to be slightly less reactive than ethane, regardless of which set of quantum yields are used. In general, the MIR and MOIR scales represent the range of conditions which are appropriate to consider when evaluating relative reactivities of VOC for control strategy purposes (Carter, 1991; 1993a,b).

However, other than considerations of precedence, the reactivity of acetone relative to ethane is of essentially no practical relevance. The two chemicals have vastly different physical properties and come from quite different types of sources, and to our knowledge no substitutions of acetone for ethane (or vise-versa) are being contemplated. If a reactive VOC is exempted, and if it is not used primarily as a substitute for more reactive VOCs, the net effect would be that there would have to be a slightly greater controls on all other (non-exempt) VOCs to achieve the same air quality gains. Thus, in effect, the proposal to exempt a VOC is equivalent to proposing to substitute it for the base ROG mixture. Therefore, the more relevant consideration when considering whether to exempt acetone is its reactivity compared to the base ROG mixture.

When compared on the basis of reactivities relative to the base ROG mixture, a somewhat different picture is obtained concerning the relative impacts of acetone and ethane on ozone formation. In particular, the relative reactivity (i.e., incremental reactivity relative to the base ROG) of acetone is found to vary over a considerably narrower range than is the case for ethane. Indeed, it is the variability of the relative reactivity of ethane, not acetone, which causes the variability of the acetone/ethane reactivity ratios among the scenarios. For example, the scenario with the most extreme acetone/ethane reactivity ratios (of 2-3) had relative reactivities for acetone very close to the average. The minimum, maximum, and average relative reactivities we obtained are summarized on Table 6, where they are compared with relative reactivities in the MIR and MOIR scales. It should be noted that the base case scenarios were designed to represent near-worst-case conditions only, and the results may be more variable if a greater variety of scenarios were included. However, these scenarios are representative of a wide variety of conditions which need to be considered when assessing effects of VOC controls.

Table 6. Summary of reactivities of acetone and ethane relative to the base ROG mixture.

	Based on effect on O_3 Yield			Based on Integrated O_3 > 0.12 ppm		
	Acetone (standard)	**Acetone (adjusted)**	**Ethane**	**Acetone (standard)**	**Acetone (adjusted)**	**Ethane**
Base case						
Minimum	0.11	0.09	0.05	0.10	0.07	0.05
Maximum	0.18	0.16	0.24	0.15	0.14	0.19
Average Base	0.14±0.01	0.13±0.02	0.17±0.04	0.12±0.01	0.10±0.01	0.12±0.03
MIR Scale	0.13	0.11	0.08			
MOIR Scale	0.14	0.12	0.15			

We believe the type of data on Table 6 provides a more appropriate basis for deciding whether it is appropriate to exempt acetone or ethane. Note that when the EPA decided to exempt ethane, in effect it decided it was not necessary to regulate emissions of a VOC which could be almost 25% asreactive as the average of all emissions in terms of peak ozone concentrations, and almost 20% as reactive in terms of effect on integrated ozone over the standard. When looked at this way, exempting a compound which is calculated to be no more than 20% as reactive in terms of peak ozone, or 15% as reactive in terms of integrated ozone over the standard, does not appear to be an inconsistent policy.

To conclude, when considering whether a VOC should be exempted from regulation as an ozone precursor, the most appropriate factor to consider is its relative reactivity, i.e., its reactivity relative to the mixture of all other VOC emissions. The results of this study indicate that the difference in relative reactivities between ethane and acetone is less than the variability of their relative reactivities from scenario to scenario. On this basis, it can be concluded the acetone and ethane can be considered to have essentially the same reactivity to within their variability with environmental conditions. However, it should be emphasized that the scenarios we employed were designed to represent near-worst-case conditions only, and the variability may be greater when considering a wider range of scenarios.

REFERENCES

Atkinson, R. and W. P. L. Carter (1984): "Kinetics and Mechanisms of the Gas-Phase Reactions of Ozone with Organic Compounds under Atmospheric Conditions," Chem. Rev. 1984, 437-470.

Atkinson, R. (1989): "Kinetics and Mechanisms of the Gas-Phase Reactions of the Hydroxyl Radical with Organic Compounds," J. Phys. Chem. Ref. Data, Monograph no 1.

Atkinson, R. (1990): "Gas-Phase Tropospheric Chemistry of Organic Compounds: A Review," Atmos. Environ., 24A, 1-24.

Atkinson, R. (1991): "Kinetics and Mechanisms of the Gas-Phase Reactions of the NO_3 Radical with Organic Compounds," J. Phys. Chem. Ref. Data, 20, 459-507.

Atkinson, R. and W. P. L. Carter (1992): "Reactions of Alkoxy Radicals under Atmospheric Conditions: The Relative Importance of Decomposition versus Reaction with O_2," J. Atm. Chem., 13, 195-210.

Atkinson, R., D. L. Baulch, R. A. Cox, R. F. Hampson, Jr., J. A. Kerr, and J. Troe (1992): "Evaluated Kinetic and Photochemical Data for Atmospheric Chemistry. Supplement IV. IUPAC Subcommittee on Gas Kinetic Data Evaluation for Atmospheric Chemistry," J. Phys. Chem. Ref. Data 21, 1125-1568.

Atkinson, R. (1993): "Gas-Phase Tropospheric Chemistry of Organic Compounds," J. Phys. Chem. Ref. Data, Monograph No. 2, in press.

Atkinson, R., S. M. Aschmann, J. Arey and B. Shorees (1992): "Formation of OH Radicals in the Gas-Phase Reactions of Ozone with a Series of Terpenes," J. Geophys. Res. 97, 6065-6073.

Atkinson, R. and S. M. Aschmann (1993): "OH Radical Production from the Gas-Phase Reactions of O_3 with a Series of Alkenes under Atmospheric Conditions," Environ. Sci. Technol, 27, 1357-1363.

Bauges, K (1990): "Preliminary Planning Information for Updating the Ozone Regulatory Impact Analysis Version of EKMA," Draft Document, Source Receptor Analysis Branch, Technical Support Division, U. S. Environmental Protection Agency, Research Triangle Park, NC, January.

Bridier, I., H. Caralp, R. Loirat, B. Lesclaux and B. Veyret (1991): "Kinetic and Theoretical Studies of the Reactions of $CH_3C(O)O_2 + NO_2 + M <=> CH_3C(O)O_2NO_2 + M$ between 248 and 393 K and between 30 and 760 Torr," J. Phys. Chem. 95, 3594-3600.

Calvert, J. G., and J. N. Pitts, Jr. (1966): Photochemistry, John Wiley and Sons, New York.

Cantrell, C. A., J. A. Davidson, A. H. McDaniel, R. E. Shetter and J. G. Calvert (1990): "Temperature-Dependent Formaldehyde Cross Sections in the Near Ultraviolet Spectral Region," J. Phys. Chem. 94, 3902-3908.

CARB (1991): "Proposed Reactivity Adjustment Factors for Transitional Low-Emissions Vehicles: Technical Support Document," California Air Resources Board, Sacramento, CA., September 27.

Carter, W. P. L., A. C. Lloyd, J. L. Sprung, and J. N. Pitts, Jr. (1979): "Computer Modeling of Smog Chamber Data: Progress in Validation of a Detailed Mechanism for the Photooxidation of Propene and n-Butane in Photochemical Smog", Int. J. Chem. Kinet, 11, 45.

Carter, W. P. L., R. Atkinson, A. M. Winer, and J. N. Pitts, Jr. (1982): "Experimental Investigation of Chamber-Dependent Radical Sources," Int. J. Chem. Kinet., 14, 1071.

Carter, W. P. L., P. S. Ripley, C. G. Smith, and J. N. Pitts, Jr. (1981): "Atmospheric Chemistry of Hydrocarbon Fuels: Vol I, Experiments, Results and Discussion," Final report to the U. S. Air Force, ESL-TR-81-53, November.

Carter, W. P. L., Dodd, M. C., Long, W. D. and Atkinson, R. (1984): Outdoor Chamber Study to Test Multi-Day Effects. Volume I: Results and Discussion. Final report, EPA-600/3-84-115, November

Carter, W. P. L., W. D. Long, L. N. Parker, and M. C. Dodd (1986): "Effects of Methanol Fuel Substitution on Multi-Day Air Pollution Episodes," Final Report on California Air Resources Board Contract No. A3-125-32, April.

Carter, W. P. L. and R. Atkinson (1987): "An Experimental Study of Incremental Hydrocarbon Reactivity," Environ. Sci. Technol., 21, 670-679

Carter, W. P. L. and R. Atkinson (1989): "A Computer Modeling Study of Incremental Hydrocarbon Reactivity", Environ. Sci. and Technol., 23, 864.

Carter, W. P. L. (1990): "A Detailed Mechanism for the Gas-Phase Atmospheric Reactions of Organic Compounds," Atm. Environ., 24A, 481-518.

Carter, W. P. L., and F. W. Lurmann (1990): "Evaluation of the RADM Gas-Phase Chemical Mechanism," Final Report, EPA-600/3-90-001.

Carter, W. P. L. (1991): "Development of Ozone Reactivity Scales for Volatile Organic Compounds", EPA-600/3-91/050, August.

Carter, W. P. L. and F. W. Lurmann (1991): "Evaluation of a Detailed Gas-Phase Atmospheric Reaction Mechanism using Environmental Chamber Data," Atm. Environ. 25A, 2771-2806.

Carter, W. P. L. (1992): "Analysis of ROG Surrogates for Environmental Chamber Studies of VOC Reactivity," interim report for CRC contract ME-9, October 15.

Carter, W. P. L. and R. Walters (1992): "Design and Specification of a Light Source for Experimental Studies of Atmospheric Reactivities of Volatile Organic Compounds," report to the National Renewable Energy Laboratory Contract No. XZ 2120751, August 15.

Carter, W. P. L. (1993a): "Development and Application of an Up-To-Date Photochemical Mechanism for Airshed Modeling and Reactivity Assessment," Draft final report for California Air Resources Board Contract No. A934-094, April 26.

Carter, W. P. L. (1993b): "Development of Ozone Reactivity Scales for Volatile Organic Compounds," Submitted to J. A&WMA, September 22.

Carter, W. P. L., J. A. Pierce, I. L. Malkina, D. Luo and W. D. Long (1993a): "Environmental Chamber Studies of Maximum Incremental Reactivities of Volatile Organic Compounds," Report to Coordinating Research Council, Project No. ME-9, California Air Resources Board Contract No. A032-0692; South Coast Air Quality Management District Contract No. C91323, United States Environmental Protection Agency Cooperative Agreement No. CR-814396-01-0, University Corporation for Atmospheric Research Contract No. 59166, and Dow Corning Corporation. April 1.

Carter, W. P. L., J. A. Pierce, D. Luo and I. L. Malkina (1993b): "Environmental Chamber Studies of Maximum Incremental Reactivities of Volatile Organic Compounds," To be submitted to Atmospheric Environment, October 4.

Croes, B. E. (1991): Technical Support Division, California Air Resources Board, personal communication.

Croes, B. E. et al. (1993): "Southern California Air Quality Study Data Archive," Research Division, California Air Resources Board.

Dasgupta, P. K, Dong, S. and Hwang, H. (1988): "Continuous Liquid Phase Fluorometry Coupled to a Diffusion Scrubber for the Determination of Atmospheric Formaldehyde, Hydrogen Peroxide, and Sulfur Dioxide," Atmos. Environ. 22, 949-963.

Dasgupta, P.K, Dong, S. and Hwang, H. (1990): Aerosol Science and Technology 12, 98-104

Dimitriades, B. (1993): U. S. Environmental Protection Agency, Atmospheric Research and Exposure Assessment Laboratory, Research Triangle Park, NC: Letter to Dr. David Morgott of Eastman Kodak Co., dated September 25.

Dodge, M. C. (1984): "Combined Effects of Organic Reactivity and NMHC/NO_x Ratio on Photochemical Oxidant Formation -- A Modeling Study," Atmos. Environ., 18, 1657.

Dong, S. and Dasgupta, P. K. (1987): "Fast Fluorometric Flow Analysis of Formaldehyde," Environ. Sci. and Technol. 21, 581-588.

Doyle, G. J., P. J. Bekowies, A. M. Winer, and J. N. Pitts, Jr. (1977): Environ. Sci. Technol. 11, 45.

Eastman Chemical Company and Hoechst Celanese Corporation (1993): "Petition for the Exemption of Acetone from Regulation under the Clean Air Act as a Precursor to Tropospheric Ozone," Petition before the U. S. Environmental Protection Agency, Latham & Watkins, Counsel, Washington DC.

EPA (1984): "Guideline for Using the Carbon Bond Mechanism in City-Specific EKMA," EPA-450/4-84-005, February.

Gardner, E. P., R. D. Wijayaratne, and J. G. Calvert (1984): "Primary Quantum Yields of Photodecomposition of Acetone in Air under Tropospheric Conditions," J. Phys. Chem. 88, 5069-5076.

Gardner, E. P., P. D. Sperry, and J. G. Calvert (1987): "Photodecomposition of Acrolein in O_2-N_2 Mixtures," J. Phys. Chem. 91, 1922.

Gery, M. W., R. D. Edmond and G. Z. Whitten (1987): "Tropospheric Ultraviolet Radiation. Assessment of Existing Data and Effects on Ozone Formation," Final Report, EPA-600/3-87-047, October.

Gery, M. W., G. Z. Whitten, and J. P. Killus (1988): "Development and Testing of the CBM-IV For Urban and Regional Modeling,", EPA-600/ 3-88-012, January.

Gery, M. W. (1991): "Review of the SAPRC-90 Chemical Mechanism," Report to the California Air Resources Board, Contract No. A132-055, Sacramento, CA.

Gipson, G. L., W. P. Freas, R. A. Kelly and E. L. Meyer (1981): "Guideline for Use of City-Specific EKMA in Preparing Ozone SIPs, EPA-450/4-80-027, March.

Gipson, G. L. and W. P. Freas (1983): "Use of City-Specific EKMA in the Ozone RIA," U. S. Environmental Protection Agency, July.

Gipson, G. L. (1984): "Users Manual for OZIPM-2: Ozone Isopleth Plotting Package With Optional Mechanism/Version 2," EPA-450/4-84-024, August.

Hogo, H. and M. W. Gery (1988): "Guidelines for Using OZIPM-4 with CBM-IV or Optional Mechanisms. Volume 1. Description of the Ozone Isopleth Plotting Package Version 4", Final Report for EPA Contract No. 68-02-4136, Atmospheric Sciences Research Laboratory, Research Triangle Park, NC. January 1988.

Jeffries, H. E. (1988): Department of Environmental Science and Engineering, University of North Carolina, Chapel Hill, NC, diskette containing JSPECTRA code and input files. Main JSPECTRA source file dated June 22. Example input files dated November 10.

Jeffries H. E., K. G. Sexton, J. R. Arnold, and T. L. Kale (1989a): "Validation Testing of New Mechanisms with Outdoor Chamber Data. Volume 2: Analysis of VOC Data for the CB4 and CAL Photochemical Mechanisms," Final Report, EPA-600/3-89-010b.

Jeffries H. E., K. G. Sexton, J. R. Arnold, and T. L. Kale (1989b): "Validation Testing of New Mechanisms with Outdoor Chamber Data. Volume 3: Calculation of Photochemical Reaction Photolysis Rates in the UNC Outdoor Chamber," Final Report, EPA-600/3-89-010c.

Jeffries, H. E. and R. Crouse (1991): "Scientific and Technical Issues Related to the Application of Incremental Reactivity. Part II: Explaining Mechanism Differences," Report prepared for Western States Petroleum Association, Glendale, CA, October.

Jeffries, H. E. (1991a): "UNC Solar Radiation Models," unpublished draft report for EPA Cooperative Agreements CR813107, CR813964 and CR815779". Undated.

Jeffries, H. E. (1991b): Department of Environmental Science and Engineering, University of North Carolina, Chapel Hill, NC, personal communication.

Jeffries, H. (1992): "Comments on CARB's Request for Waiver of Federal Preemption in CAAA," Presented at the EPA Public Hearing for California ARB's Request for Waiver of Waiver of Federal Preemption.

Jeffries, H. E., M. W. Gery and W. P. L. Carter (1992): "Protocol for Evaluating Oxidant Mechanisms for Urban and Regional Models," Report for U. S. Environmental Protection Agency Cooperative Agreement No. 815779, Atmospheric Research and Exposure Assessment Laboratory, Research Triangle Park, NC.

Jeffries, H. E. (1993): Department of Environmental Science and Engineering, University of North Carolina, Chapel Hill, NC, communication to J. J. Bufalini, U. S. Environmental Protection Agency, Atmospheric Research and Exposure Assessment Laboratory, Research Triangle Park, NC.

Jenkin, M. E., R. A. Cox, M. Emrich and G. K. Moortgat (1993): "Mechanisms for the Cl-atom-initiated Oxidation of Acetone and Hydroxyacetone in Air," J. Chem. Soc. Faraday Trans. 89, 2983-2991.

Johnson, G. M. (1983): "Factors Affecting Oxidant Formation in Sydney Air," in "The Urban Atmosphere -- Sydney, a Case Study." Eds. J. N. Carras and G. M. Johnson (CSIRO, Melbourne), pp. 393-408.

Lurmann, F. W., H. H. Main, K. T. Knapp, L. Stockburrger, R. A. Rasmussen and K. Fung (1992): "Analysis of Ambient VOC Data Collected in the Southern California Air Quality Study," Final Report to California Air Resources Board Contract No. A382-130; Research Division, Sacramento, CA, February.

Meyrahn, H., J. Pauly, W. Schneider, and P. Warneck (1986): "Quantum Yields for the Photodissociation of Acetone in Air and an Estimate for the Life Time of Acetone in the Lower Troposphere," J. Atmos. Chem. 4, 277-291.

Rogers, J. D. (1990): "Ultraviolet Absorption Cross Sections and Atmospheric Photodissociation Rate Constants of Formaldehyde," J. Phys. Chem., 90, 4011-4015.

Tuazon, E. C., W. P. L. Carter and R. Atkinson (1991): "Thermal Decomposition of Peroxyacetyl Nitrate and Reactions of Acetyl Peroxy Radicals with NO and NO_2 Over the Temperature Range 283-313 K," J. Phys. Chem., in 95, 2434.

Zafonte, L., P. L. Rieger, and J. R. Holmes (1977): "Nitrogen Dioxide Photolysis in the Los Angeles Atmosphere," Environ. Sci. Technol. 11, 483-487.

APPENDIX A.
LISTING OF THE UPDATED SAPRC MECHANISM

A complete listing of the updated SAPRC used in this study is given in Tables A-1 through A-3. Table A-1 gives a list of the model species, Table A-2 gives the reactions, and Table A-3 gives the absorption cross sections and quantum yields used to calculate the photolysis rates.

Table A-1. List of model species used in the SAPRC-93 mechanism for the base case simulations.

name	description
Constant Species.	
O2	Oxygen
M	Air
H2O	Water
Active Inorganic Species.	
O3	Ozone
NO	Nitric Oxide
NO2	Nitrogen Dioxide
NO3	Nitrate Radical
N2O5	Nitrogen Pentoxide
HONO	Nitrous Acid
HNO3	Nitric Acid
HNO4	Peroxynitric Acid
HO2H	Hydrogen Peroxide
Active Radical Species and Operators.	
HO2.	Hydroperoxide Radicals
RO2.	Operator to Calculate Total Organic Peroxy Radicals
RCO3.	Operator to Calculate Total Acetyl Peroxy Radicals
Active Reactive Organic Product Species.	
CO	Carbon Monoxide
HCHO	Formaldehyde
CCHO	Acetaldehyde
RCHO	Lumped C3+ Aldehydes
ACET	Acetone
MEK	Lumped Ketones
PHEN	Phenol
CRES	Cresols

Table A-1, (continued)

Name	Description
BALD	Aromatic aldehydes (e.g., benzaldehyde)
GLY	Glyoxal
MGLY	Methyl Glyoxal
AFG1	Reactive Aromatic Fragmentation Products from benzene and naphthalene
AFG2	Other Reactive Aromatic Fragmentation Products
AFG3	Aromatic Fragmentation Products used in adjusted m-xylene mechanism
RNO3	Organic Nitrates
NPHE	Nitrophenols
PAN	Peroxy Acetyl Nitrate
PPN	Peroxy Propionyl Nitrate
GPAN	PAN Analogue formed from Glyoxal
PBZN	PAN Analogues formed from Aromatic Aldehydes
-OOH	Operator Representing Hydroperoxy Groups
Non-Reacting Species	
CO2	Carbon Dioxide
-C	"Lost Carbon"
-N	"Lost Nitrogen"
H2	Hydrogen
Steady State Species and Operators.	
HO.	Hydroxyl Radicals
O	Ground State Oxygen Atoms
O*1D2	Excited Oxygen Atoms
RO2-R.	Peroxy Radical Operator representing NO to NO_2 conversion with HO_2 formation.
RO2-N.	Peroxy Radical Operator representing NO consumption with organic nitrate formation.
RO2-NP.	Peroxy Radical Operator representing NO consumption with nitrophenol formation
R2O2.	Peroxy Radical Operator representing NO to NO_2 conversion.
CCO-O2.	Peroxy Acetyl Radicals
C2CO-O2.	Peroxy Propionyl Radicals
HCOCO-O2.	Peroxyacyl Radical formed from Glyoxal
BZ-CO-O2.	Peroxyacyl Radical formed from Aromatic Aldehydes
HOCOO.	Intermediate formed in Formaldehyde + HO_2 reaction
BZ-O.	Phenoxy Radicals
BZ(NO2)-O.	Nitratophenoxy Radicals
HOCOO.	Radical Intermediate formed in the HO_2 + Formaldehyde system.
(HCHO2)	Excited Criegee biradicals formed from $=CH_2$ groups
(CCHO2)	Excited Criegee biradicals formed from $=CHCH_3$ groups
(RCHO2)	Excited Criegee biradicals formed from =CHR groups, where R not CH_3
(C(C)CO2)	Excited Criegee biradicals formed from $=C(CH_3)_2$ groups
(C(R)CO2)	Excited Criegee biradicals formed from $=C(CH_3)R$ or CR_2 groups
(BZCHO2)	Excited Criegee biradicals formed from styrenes

Table A-1, (continued)

Name	Description
Hydrocarbon species represented explicitly	
CH4	Methane (EKMA simulations only)
ETHANE	Ethane (Ethane reactivity simulations only)
N-C4	n-Butane (Chamber simulations only)
N-C6	n-Hexane (Chamber simulations only)
N-C8	n-Octane (Chamber simulations only)
ETHE	Ethene
ISOP	Isoprene (EKMA Simulations only)
APIN	α-Pinene (EKMA Simulations only)
UNKN	Unknown biogenics. (EKMA Simulations only)
PROPENE	Propene (Chamber simulations only)
T-2-BUTE	trans-2-Butene (Chamber simulations only)
TOLUENE	Toluene (Chamber simulations only)
M-XYLENE	m-Xylene (Chamber simulations only)
Lumped alkane and aromatic species used to represent the Base ROG mixture in the EKMA model simulations.	
AAR1	Alkanes and aromatics with $k_{OH} < 5x10^3$ ppm^{-1} min^{-1}
AAR2	Alkanes and aromatics with k_{OH} between $5x10^3$ and $1.5x10^4$ ppm^{-1} min^{-1}
AAR3	Alkanes and aromatics with $k_{OH} > 1.5x10^4$ ppm^{-1} min^{-1}
Lumped higher alkenes used to represent the Base ROG mixture in the EKMA model simulations	
OLE2	Alkenes with $k_{OH} < 7x10^4$ ppm^{-1} min^{-1} (Primarily terminal alkenes.)
OLE3	Alkenes with $k_{OH} > 7x10^4$ ppm^{-1} min^{-1} (Primary internal alkenes.)

Table A-2. Listing of SAPRC-93 mechanism as used to in the base case simulations.

Rxn. Label	Kinetic Parameters [a] k(300)	A	Ea	B	Reactions [b]
Inorganic Reactions					
1	(Phot. Set = NO2)				NO2 + HV = NO + O
2	2.16E-05	2.16E-05	0.00	-4.30	O + O2 + M = O3 + M
3A	1.42E+04	9.54E+03	-0.24	-1.00	O + NO2 = NO + O2
3B	2.28E+03	(Falloff Kinetics)			O + NO2 = NO3 + M
	k0 =	3.23E-03	0.00	-4.00	
	kINF =	3.23E+04	0.00	-1.00	
		F= 0.60	n= 1.00		
4	2.76E+01	2.94E+03	2.78	-1.00	O3 + NO = NO2 + O2
5	4.94E-02	2.06E+02	4.97	-1.00	O3 + NO2 = O2 + NO3
6	4.11E+04	2.49E+04	-0.30	-1.00	NO + NO3 = #2 NO2
7	6.90E-10	1.19E-10	-1.05	-2.00	NO + NO + O2 = #2 NO2
8	1.84E+03	(Falloff Kinetics)			NO2 + NO3 = N2O5
	k0 =	7.90E-02	0.00	-6.30	
	kINF =	2.20E+03	0.00	-1.50	
		F= 0.60	n= 1.00		
9	2.26E-03	3.72E+13	22.26	1.00	N2O5 + #RCON8 = NO2 + NO3
10	1.47E-06	1.47E-06	0.00	-1.00	N2O5 + H2O = #2 HNO3
11	6.13E-01	3.67E+01	2.44	-1.00	NO2 + NO3 = NO + NO2 + O2
12A	(Phot. Set = NO3NO)				NO3 + HV = NO + O2
12B	(Phot. Set = NO3NO2)				NO3 + HV = NO2 + O
13A	(Phot. Set = O3O3P)				O3 + HV = O + O2
13B	(Phot. Set = O3O1D)				O3 + HV = O*1D2 + O2
14	3.23E+05	3.23E+05	0.00	-1.00	O*1D2 + H2O = #2 HO.
15	4.29E+04	2.82E+04	-0.25	-1.00	O*1D2 + M = O + M
16	7.05E+03	(Falloff Kinetics)			HO. + NO = HONO
	k0 =	2.51E-02	0.00	-4.60	
	kINF =	2.20E+04	0.00	-1.50	
		F= 0.60	n= 1.00		
17	(Phot. Set = HONO)				HONO + HV = HO. + NO
18	1.66E+04	(Falloff Kinetics)			HO. + NO2 = HNO3
	k0 =	9.34E-02	0.00	-5.20	
	kINF =	3.52E+04	0.00	-2.30	
		F= 0.60	n= 1.00		
19	1.51E+02	9.47E+00	-1.65	-1.00	HO. + HNO3 = H2O + NO3
21	3.52E+02	3.52E+02	0.00	-1.00	HO. + CO = HO2. + CO2
22	1.02E+02	2.35E+03	1.87	-1.00	HO. + O3 = HO2. + O2
23	1.21E+04	5.43E+03	-0.48	-1.00	HO2. + NO = HO. + NO2
24	2.00E+03	(Falloff Kinetics)			HO2. + NO2 = HNO4
	k0 =	6.46E-03	0.00	-5.20	
	kINF =	6.90E+03	0.00	-2.40	
		F= 0.60	n= 1.00		
25	3.24E-03	1.95E+13	21.66	1.00	HNO4 + #RCON24 = HO2. + NO2
27	6.77E+03	1.91E+03	-0.75	-1.00	HNO4 + HO. = H2O + NO2 + O2
28	3.05E+00	1.61E+01	0.99	-1.00	HO2. + O3 = HO. + #2 O2
29A	2.54E+03	3.23E+02	-1.23	-1.00	HO2. + HO2. = HO2H + O2
29B	1.80E-03	6.82E-05	-1.95	-2.00	HO2. + HO2. + M = HO2H + O2
29C	1.34E-01	1.11E-05	-5.60	-2.00	HO2. + HO2. + H2O = HO2H + O2 + H2O
29D	9.52E-02	2.37E-06	-6.32	-2.00	HO2. + HO2. + H2O = HO2H + O2 + H2O
30A	(Same k as Reaction 29A)				NO3 + HO2. = HNO3 + O2
30B	(Same k as Reaction 29B)				NO3 + HO2. + M = HNO3 + O2
30C	(Same k as Reaction 29C)				NO3 + HO2. + H2O = HNO3 + O2 + H2O
30D	(Same k as Reaction 29D)				NO3 + HO2. + H2O = HNO3 + O2 + H2O
31	(Phot. Set = H2O2)				HO2H + HV = #2 HO.
32	2.49E+03	4.84E+03	0.40	-1.00	HO2H + HO. = HO2. + H2O
33	1.45E+05	6.75E+04	-0.46	-1.00	HO. + HO2. = H2O + O2
Peroxy Radical Operators					
B1	1.13E+04	6.16E+03	-0.36	-1.00	RO2. + NO = NO
B2	3.31E+04	(Falloff Kinetics)			RCO3. + NO = NO
	k0 =	2.03E+01	0.00	-9.10	
	kINF =	3.87E+04	0.00	-1.90	
		F= 0.27	n= 1.00		
B4	1.52E+04	(Falloff Kinetics)			RCO3. + NO2 = NO2
	k0 =	9.23E+00	0.00	-9.10	
	kINF =	1.76E+04	0.00	-1.90	
		F= 0.30	n= 1.00		
B5	7.19E+03	4.99E+02	-1.59	-1.00	RO2. + HO2. = HO2. + RO2-HO2-PROD
B6	7.19E+03	4.99E+02	-1.59	-1.00	RCO3. + HO2. = HO2. + RO2-HO2-PROD
B8	1.47E+00	1.47E+00	0.00	-1.00	RO2. + RO2. = RO2-RO2-PROD
B9	1.60E+04	2.73E+03	-1.05	-1.00	RO2. + RCO3. = RO2-RO2-PROD
B10	2.40E+04	4.11E+03	-1.05	-1.00	RCO3. + RCO3. = RO2-RO2-PROD
B11	(Same k as Reaction B1)				RO2-R. + NO = NO2 + HO2.
B12	(Same k as Reaction B5)				RO2-R. + HO2. = -OOH
B13	(Same k as Reaction B8)				RO2-R. + RO2. = RO2. + #.5 HO2.
B14	(Same k as Reaction B9)				RO2-R. + RCO3. = RCO3. + #.5 HO2.

Table A-2 (continued)

Rxn. Label	Kinetic Parameters [a] k(300)	A	Ea	B	Reactions [b]
B19	(Same k as Reaction B1)				RO2-N. + NO = RNO3
B20	(Same k as Reaction B5)				RO2-N. + HO2. = -OOH + MEK + #1.5 -C
B21	(Same k as Reaction B8)				RO2-N. + RO2. = RO2. + #.5 HO2. + MEK + #1.5 -C
B22	(Same k as Reaction B9)				RO2-N. + RCO3. = RCO3. + #.5 HO2. + MEK + #1.5 -C
B15	(Same k as Reaction B1)				R2O2. + NO = NO2
B16	(Same k as Reaction B5)				R2O2. + HO2. =
B17	(Same k as Reaction B8)				R2O2. + RO2. = RO2.
B18	(Same k as Reaction B9)				R2O2. + RCO3. = RCO3.
B23	(Same k as Reaction B1)				RO2-XN. + NO = -N
B24	(Same k as Reaction B5)				RO2-XN. + HO2. = -OOH
B25	(Same k as Reaction B8)				RO2-XN. + RO2. = RO2. + #.5 HO2.
B26	(Same k as Reaction B9)				RO2-XN. + RCO3. = RCO3. + HO2.
G2	(Same k as Reaction B1)				RO2-NP. + NO = NPHE
G3	(Same k as Reaction B5)				RO2-NP. + HO2. = -OOH + #6 -C
G4	(Same k as Reaction B8)				RO2-NP. + RO2. = RO2. + #.5 HO2. + #6 -C
G5	(Same k as Reaction B9)				RO2-NP. + RCO3. = RCO3. + HO2. + #6 -C
Excited Criegee Biradicals					
RZ1	6.00E+01	(No T Dependence)			(HCHO2) = #.12 CO + #.18 CO2 + #.7 HCOOH + #.12 HO2. + #.12 HO.
RZ2	6.00E+01	(No T Dependence)			(CCHO2) = #.25 CCOOH + #.15 "CH4 + CO2" + #.6 HO. + #.3 "CCO-O2. + RCO3." + #.1 "RO2-R. + HCHO + CO + RO2."
RZ3	6.00E+01	(No T Dependence)			(RCHO2) = #.25 CCOOH + #.15 CO2 + #.6 HO. + #.3 "C2CO-O2. + RCO3." + #.1 "RO2-R. + CCHO + CO + RO2." + #.55 -C
RZ4	6.00E+01	(No T Dependence)			(C(C)CO2) = HO. + R2O2. + HCHO + CCO-O2. + RCO3. + RO2.
RZ5	6.00E+01	(No T Dependence)			(C(R)CO2) = HO. + CCO-O2. + CCHO + R2O2. + RCO3. + RO2.
RZ8	6.00E+01	(No T Dependence)			(BZCHO2) = #.5 O3OL-SB + #.5 "BZ-O. + R2O2. + CO + HO."
Lumped Hydroperoxide Group					
B7	(Phot. Set = CO2H)				-OOH + HV = HO2. + HO.
B7A	2.65E+03	1.73E+03	-0.25	-1.00	HO. + -OOH = HO.
B7B	5.45E+03	2.63E+03	-0.44	-1.00	HO. + -OOH = RO2-R. + RO2.
Formaldehyde					
C1	(Phot. Set = HCHONEWR)				HCHO + HV = #2 HO2. + CO
C2	(Phot. Set = HCHONEWM)				HCHO + HV = H2 + CO
C3	1.43E+04	1.65E+03	-1.29	1.00	HCHO + HO. = HO2. + CO + H2O
C4	1.14E+02	1.42E+01	-1.24	-1.00	HCHO + HO2. = HOCOO.
C4A	1.06E+04	1.44E+14	13.91	0.00	HOCOO. = HO2. + HCHO
C4B	(Same k as Reaction B1)				HOCOO. + NO = -C + NO2 + HO2.
C9	9.36E-01	4.11E+03	5.00	-1.00	HCHO + NO3 = HNO3 + HO2. + CO
Acetaldehyde and PAN					
C10	2.30E+04	8.15E+03	-0.62	-1.00	CCHO + HO. = CCO-O2. + H2O + RCO3.
C11A	(Phot. Set = CCHOR)				CCHO + HV = CO + HO2. + HCHO + RO2-R. + RO2.
C12	4.17E+00	2.05E+03	3.70	-1.00	CCHO + NO3 = HNO3 + CCO-O2. + RCO3.
C13	(Same k as Reaction B2)				CCO-O2. + NO = CO2 + NO2 + HCHO + RO2-R. + RO2.
C14	(Same k as Reaction B4)				CCO-O2. + NO2 = PAN
C15	(Same k as Reaction B6)				CCO-O2. + HO2. = -OOH + CO2 + HCHO
C16	(Same k as Reaction B9)				CCO-O2. + RO2. = RO2. + #.5 HO2. + CO2 + HCHO
C17	(Same k as Reaction B10)				CCO-O2. + RCO3. = RCO3. + HO2. + CO2 + HCHO
C18	3.90E-02	(Falloff Kinetics)			PAN = CCO-O2. + NO2 + RCO3.
	k0 =	7.19E+12	23.97	-1.00	
	kINF =	2.40E+18	27.08	0.00	
		F= 0.30	n= 1.00		
C3+ Aldehydes and PPN					
C25	2.89E+04	1.25E+04	-0.50	-1.00	RCHO + HO. = C2CO-O2. + RCO3.
C26	(Phot. Set = RCHO)				RCHO + HV = CCHO + RO2-R. + RO2. + CO + HO2.
C27	4.17E+00	2.05E+03	3.70	-1.00	NO3 + RCHO = HNO3 + C2CO-O2. + RCO3.
C28	(Same k as Reaction B2)				C2CO-O2. + NO = CCHO + RO2-R. + CO2 + NO2 + RO2.
C29	1.23E+04	1.23E+04	0.00	-1.00	C2CO-O2. + NO2 = PPN
C30	(Same k as Reaction B6)				C2CO-O2. + HO2. = -OOH + CCHO + CO2
C31	(Same k as Reaction B9)				C2CO-O2. + RO2. = RO2. + #.5 HO2. + CCHO + CO2
C32	(Same k as Reaction B10)				C2CO-O2. + RCO3. = RCO3. + HO2. + CCHO + CO2
C33	4.07E-02	9.60E+18	27.97	0.00	PPN = C2CO-O2. + NO2 + RCO3.

Table A-2 (continued)

Rxn. Label	Kinetic Parameters [a] k(300)	A	Ea	B	Reactions [b]
Acetone (standard mechanism)					
C38	3.28E+02	7.06E+02	0.46	1.00	ACET + HO. = R2O2. + HCHO + CCO-O2. + RCO3. + RO2.
C39	(Phot. Set = ACET-93C)				ACET + HV = CCO-O2. + HCHO + RO2-R. + RCO3. + RO2.
Acetone (adjusted mechanism)					
C38	3.28E+02	7.06E+02	0.46	1.00	ACET + HO. = R2O2. + HCHO + CCO-O2. + RCO3. + RO2.
C39x	(Phot. Set = ADJACET)				ACET + HV = CCO-O2. + HCHO + RO2-R. + RCO3. + RO2.
C4+ Ketones					
C44	1.70E+03	4.29E+02	-0.82	1.00	MEK + HO. = H2O + #.5 "CCHO + HCHO + CCO-O2. + C2CO-O2." + RCO3. + #1.5 "R2O2. + RO2."
C57	(Phot. Set = KETONE)				MEK + HV + #.1 = CCO-O2. + CCHO + RO2-R. + RCO3. + RO2.
Organic Nitrates					
C95	3.03E+03	3.22E+04	1.41	-1.00	RNO3 + HO. = NO2 + #.155 MEK + #1.05 RCHO + #.48 CCHO + #.16 HCHO + #.11 -C + #1.39 "R2O2. + RO2."
Glyoxal and GPAN					
C58A	(Phot. Set = GLYOXAL1)				GLY + HV = #.8 HO2. + #.45 HCHO + #1.55 CO
C58B	(Phot. Set = GLYOXAL2)				GLY + HV + #0.029 = #.13 HCHO + #1.87 CO
C59	1.67E+04	1.67E+04	0.00	-1.00	GLY + HO. = #.6 HO2. + #1.2 CO + #.4 "HCOCO-O2. + RCO3."
C60	(Same k as Reaction C12)				GLY + NO3 = HNO3 + #.6 HO2. + #1.2 CO + #.4 "HCOCO-O2. + RCO3."
C62	(Same k as Reaction B2)				HCOCO-O2. + NO = NO2 + CO2 + CO + HO2.
C63	(Same k as Reaction B4)				HCOCO-O2. + NO2 = GPAN
C65	(Same k as Reaction B6)				HCOCO-O2. + HO2. = -OOH + CO2 + CO
C66	(Same k as Reaction B9)				HCOCO-O2. + RO2. = RO2. + #.5 HO2. + CO2 + CO
C67	(Same k as Reaction B10)				HCOCO-O2. + RCO3. = RCO3. + HO2. + CO2 + CO
C64	(Same k as Reaction C18)				GPAN = HCOCO-O2. + NO2 + RCO3.
Methyl Glyoxal					
C68A	(Phot. Set = MEGLYOX1)				MGLY + HV = HO2. + CO + CCO-O2. + RCO3.
C68B	(Phot. Set = MEGLYOX2)				MGLY + HV + #.107 = HO2. + CO + CCO-O2. + RCO3.
C69	2.52E+04	2.52E+04	0.00	-1.00	MGLY + HO. = CO + CCO-O2. + RCO3.
C70	(Same k as Reaction C12)				MGLY + NO3 = HNO3 + CO + CCO-O2. + RCO3.
Phenol and cresols					
G46	3.86E+04	3.86E+04	0.00	-1.00	HO. + PHEN = #.15 RO2-NP. + #.85 RO2-R. + #.2 GLY + #4.7 -C + RO2.
G51	5.28E+03	5.28E+03	0.00	-1.00	NO3 + PHEN = HNO3 + BZ-O.
G52	6.16E+04	6.16E+04	0.00	-1.00	HO. + CRES = #.15 RO2-NP. + #.85 RO2-R. + #.2 MGLY + #5.5 -C + RO2.
G57	3.08E+04	3.08E+04	0.00	-1.00	NO3 + CRES = HNO3 + BZ-O. + -C
Benzaldehyde and PBzN					
G30	1.89E+04	1.89E+04	0.00	-1.00	BALD + HO. = BZ-CO-O2. + RCO3.
G31	(Phot. Set = BZCHO)				BALD + HV + #.05 = #7 -C
G32	3.83E+00	2.05E+03	3.75	-1.00	BALD + NO3 = HNO3 + BZ-CO-O2.
G33	(Same k as Reaction B2)				BZ-CO-O2. + NO = BZ-O. + CO2 + NO2 + R2O2. + RO2.
G34	1.23E+04	1.23E+04	0.00	-1.00	BZ-CO-O2. + NO2 = PBZN
G36	(Same k as Reaction B6)				BZ-CO-O2. + HO2. = -OOH + CO2 + PHEN
G37	(Same k as Reaction B9)				BZ-CO-O2. + RO2. = RO2. + #.5 HO2. + CO2 + PHEN
G38	(Same k as Reaction B10)				BZ-CO-O2. + RCO3. = RCO3. + HO2. + CO2 + PHEN
G35	1.30E-02	9.60E+16	25.90	0.00	PBZN = BZ-CO-O2. + NO2 + RCO3.
Nitrophenols					
G58	5.28E+03	5.28E+03	0.00	-1.00	NPHE + NO3 = HNO3 + BZ(NO2)-O.
G43	5.19E+04	1.91E+04	-0.60	-1.00	BZ-O. + NO2 = NPHE
G44	(Same k as Reaction B5)				BZ-O. + HO2. = PHEN
G45	6.00E-02	(No T Dependence)			BZ-O. = PHEN
G59	(Same k as Reaction G43)				BZ(NO2)-O. + NO2 = #2 -N + #6 -C
G60	(Same k as Reaction B5)				BZ(NO2)-O. + HO2. = NPHE
G61	(Same k as Reaction G45)				BZ(NO2)-O. = NPHE
Aromatic Fragmentation Products					
G7	1.67E+04	1.67E+04	0.00	-1.00	HO. + AFG1 = HCOCO-O2. + RCO3.
G8	(Phot. Set = ACROLEIN)				AFG1 + HV + #0.029 = HO2. + HCOCO-O2. + RCO3.

Table A-2 (continued)

Rxn. Label	Kinetic Parameters [a] k(300)	A	Ea	B	Reactions [b]
U2OH	2.52E+04	2.52E+04	0.00	-1.00	HO. + AFG2 = C2CO-O2. + RCO3.
U2HV	(Phot. Set = ACROLEIN)				AFG2 + HV + #0.615 = HO2. + CO + CCO-O2. + RCO3.
U3OH	2.52E+04	2.52E+04	0.00	-1.00	HO. + AFG3 = C2CO-O2. + RCO3.
U3HV	(Phot. Set = ACROLEIN)				AFG3 + HV + #0.022 = HO2. + CO + CCO-O2. + RCO3.
Methane – Used in EKMA Simulations					
RCH4	1.28E+01	9.18E+02	2.55	1.00	CH4 + HO. = HCHO + RO2-R. + RO2.
Ethane – Used for Ethane Reactivity Simulations					
OH01	2.74E-13	1.28E-12	0.92	2.00	ETHANE + HO. = RO2-R. + CCHO + RO2.
n-Butane – Used in Full Surrogate Experiment Simulations					
OH02	2.56E-12	1.36E-12	-0.38	2.00	N-C4 + HO. = #.076 RO2-N. + #.924 RO2-R. + #.397 R2O2. + #.001 HCHO + #.571 CCHO + #.14 RCHO + #.533 MEK + #-0.076 -C + #1.397 RO2.
n-Hexane – Used in Mini-Surrogate Experiment Simulations					
OH03	5.63E-12	1.35E-11	0.52	0.00	N-C6 + HO. = #.185 RO2-N. + #.815 RO2-R. + #.738 R2O2. + #.02 CCHO + #.105 RCHO + #1.134 MEK + #.186 -C + #1.738 RO2.
n-Octane – Used in Full Surrogate Experiment Simulations					
OH04	8.76E-12	3.15E-11	0.76	0.00	N-C8 + HO. = #.333 RO2-N. + #.667 RO2-R. + #.706 R2O2. + #.002 RCHO + #1.333 MEK + #.998 -C + #1.706 RO2.
Ethene					
OH05	8.43E-12	1.96E-12	-0.87	0.00	ETHENE + HO. = RO2-R. + RO2. + #1.56 HCHO + #.22 CCHO
O305	1.68E-18	9.14E-15	5.13	0.00	ETHENE + O3 = HCHO + (HCHO2)
N305	2.15E-16	5.43E-12	6.04	0.00	ETHENE + NO3 = R2O2. + RO2. + #2 HCHO + NO2
OA05	7.42E-13	1.04E-11	1.57	0.00	ETHENE + O = RO2-R. + HO2. + RO2. + HCHO + CO + #2 OLE-RI
Propene – Used in Full Surrogate Experiment Simulations					
OH06	2.60E-11	4.85E-12	-1.00	0.00	PROPENE + HO. = RO2-R. + RO2. + HCHO + CCHO
O306	1.05E-17	5.51E-15	3.73	0.00	PROPENE + O3 = #.6 HCHO + #.4 CCHO + #.4 (HCHO2) + #.6 (CCHO2)
N306	9.80E-15	4.85E-12	3.70	0.00	PROPENE + NO3 = R2O2. + RO2. + HCHO + CCHO + NO2
OA06	4.01E-12	1.18E-11	0.64	0.00	PROPENE + O = #.4 HO2. + #.5 RCHO + #.5 MEK + #-0.5 -C + #.4 OLE-RI
trans-2-Butene – Used in Full Surrogate Experiment Simulations					
OH07	6.30E-11	1.01E-11	-1.09	0.00	T-2-BUTE + HO. = RO2-R. + RO2. + #2 CCHO
O307	1.95E-16	6.64E-15	2.10	0.00	T-2-BUTE + O3 = CCHO + (CCHO2)
N307	3.92E-13	1.10E-13	-0.76	2.00	T-2-BUTE + NO3 = R2O2. + RO2. + #2 CCHO + NO2
OA07	2.34E-11	2.26E-11	-0.02	0.00	T-2-BUTE + O = #.4 HO2. + #.5 RCHO + #.5 MEK + #.5 -C + #.4 OLE-RI
Toluene – Used in Full Surrogate Experiment Simulations					
OH08	5.91E-12	1.81E-12	-0.70	0.00	TOLUENE + HO. = #.085 BALD + #.26 CRES + #.118 GLY + #.131 MGLY + #.49 AFG2 + #.74 RO2-R. + #.26 HO2. + #2.486 -C + #.74 RO2.
m-Xylene (Standard Mechanism) – Used in Full Surrogate Experiment Simulations					
OH09	2.36E-11	(No T Dependence)			M-XYLENE + HO. = #.04 BALD + #.18 CRES + #.108 GLY + #.37 MGLY + #.75 AFG2 + #.82 RO2-R. + #.18 HO2. + #2.884 -C + #.82 RO2.
m-Xylene (Adjusted Mechanism) – Used in Set 3 Mini-Surrogate Experiment Simulations (see Carter et al., 1993)					
OH09x	2.36E-11	(No T Dependence)			M-XYLENE + HO. = #.04 BALD + #.18 CRES + #.108 GLY + #.37 MGLY + #2 AFG3 + #.82 RO2-R. + #.18 HO2. + #-0.866 -C + #.82 RO2.
Isoprene (SAPRC-90 mechanism) – Used in EKMA Simulations					
ISOH	1.46E+05	3.73E+04	-0.81	-1.00	ISOP + HO. = RO2-R. + HCHO + RCHO + RO2. + -C
ISO3	2.20E-02	1.81E+01	4.00	-1.00	ISOP + O3 = #.5 HCHO + #.15 CCHO + #.5 RCHO + #.21 MEK + #.295 CO + #.285 O3OL-SB + #.165 HO2. + #.06 HO. + #.135 RO2-R. + #.135 RO2. + #1.565 -C + #.36 OLE-RI
ISN3	1.01E+03	4.45E+03	0.89	-1.00	ISOP + NO3 = NO2 + R2O2. + HCHO + RCHO + RO2. + -C
ISOA	8.81E+04	8.81E+04	0.00	-1.00	ISOP + O = #.4 HO2. + #.5 MEK + #.5 RCHO + #1.5 -C + #.4 OLE-RI
α-Pinene (SAPRC-90 mechanism) – Used in EKMA Simulations					
APOH	7.80E+04	1.78E+04	-0.88	-1.00	APIN + HO. = RO2-R. + RCHO + RO2. + #7 -C
APO3	1.47E-01	1.45E+00	1.37	-1.00	APIN + O3 = #.05 HCHO + #.2 CCHO + #.5 RCHO + #.61 MEK + #.075 CO + #.1 O3OL-SB + #.05 CCO-O2. + #.05 C2CO-O2. + #.1 RCO3. +

Table A-2 (continued)

Rxn. Label	Kinetic Parameters [a] k(300)	A	Ea	B	Reactions [b]
					#.105 HO2. + #.16 HO. + #.135 RO2-R. + #.15 R2O2. + #.285 RO2. + #5.285 -C + #.5 OLE-RI
APN3	8.95E+03	1.75E+03	-0.97	-1.00	APIN + NO3 = NO2 + R2O2. + RCHO + RO2. + #7 -C
APOA	4.40E+04	4.40E+04	0.00	-1.00	APIN + O = #.4 HO2. + #.5 MEK + #.5 RCHO + #6.5 -C + #.4 OLE-RI
Unknown Biogenics (Averaged parameters of α-pinene and β-pinene, SAPRC-90 mechanism) – Used in EKMA Simulations					
UNOH	9.64E+04	9.64E+04	0.00	-1.00	UNKN + HO. = RO2-R. + RO2. + #.5 HCHO + RCHO + #6.5 -C
UNO3	8.59E-02	8.59E-02	0.00	-1.00	UNKN + O3 = #.135 RO2-R. + #.135 HO2. + #.075 R2O2. + #.21 RO2. + #.025 CCO-O2. + #.025 C2CO-O2. + #.05 RCO3. + #.275 HCHO + #.175 CCHO + #.5 RCHO + #.41 MEK + #.185 CO + #5.925 -C + #.11 HO. + #.192 O3OL-SB + #.43 OLE-RI
UNN3	6.31E+03	6.31E+03	0.00	-1.00	UNKN + NO3 = R2O2. + RO2. + #.5 HCHO + RCHO + #6.5 -C + NO2
UNOA	4.26E+04	4.26E+04	0.00	-1.00	UNKN + O = #.4 HO2. + #.5 RCHO + #.5 MEK + #6.5 -C + #.4 OLE-RI
Representation of Alkanes and Aromatics the base ROG mixture in the EKMA simulations. [d,e]					
A1OH	2.90E+03	4.17E+03	0.22	0.00	AAR1 + HO. = #.917 RO2-R. + #.042 RO2-N. + #.007 RO2-XN. + #.034 HO2. + #.33 R2O2. + #1.295 RO2. + #.141 HCHO + #.315 CCHO + #.163 RCHO + #.254 ACET + #.25 MEK + #.024 CO + #.01 PHEN + #.065 GLY + #.077 AFG1 + #.078 -C
A2OH	8.75E+03	3.60E+03	-0.53	0.00	AAR2 + HO. = #.828 RO2-R. + #.109 RO2-N. + #.002 RO2-XN. + #.061 HO2. + #.635 R2O2. + #1.574 RO2. + #.013 HCHO + #.173 CCHO + #.205 RCHO + #.179 ACET + #.592 MEK + #.032 CO + #.007 CO2 + #.061 CRES + #.02 BALD + #.028 GLY + #.031 MGLY + #.115 AFG2 + #.917 -C
A3OH	4.30E+04	1.66E+04	-0.57	0.00	AAR3 + HO. = #.785 RO2-R. + #.079 RO2-N. + #.136 HO2. + #.198 R2O2. + #1.063 RO2. + #.003 HCHO + #.01 CCHO + #.046 RCHO + #.3 MEK + #.002 CO2 + #.136 CRES + #.027 BALD + #.046 GLY + #.36 MGLY + #.565 AFG2 + #3.376 -C
Representation of Anthropogenic C_{3+} Alkenes the base ROG mixture in the EKMA simulations. [d]					
O2OH	4.69E+04	3.28E+03	-1.59	0.00	OLE2 + HO. = #.859 RO2-R. + #.141 RO2-N. + RO2. + #.859 HCHO + #.252 CCHO + #.607 RCHO + #1.269 -C
O2O3	1.59E-02	2.10E+00	2.91	0.00	OLE2 + O3 = #.6 HCHO + #.635 RCHO + #.981 -C + #.4 (HCHO2) + #.529 (CCHO2) + #.071 (RCHO2)
O2N3	1.77E+01	3.28E+03	3.12	0.00	OLE2 + NO3 = R2O2. + RO2. + HCHO + #.294 CCHO + #.706 RCHO + #1.451 -C + NO2
O2OA	6.07E+03	6.67E+03	0.06	0.00	OLE2 + O = #.4 HO2. + #.5 RCHO + #.5 MEK + #1.657 -C + #.4 OLE-RI
O3OH	9.73E+04	7.33E+03	-1.54	0.00	OLE3 + HO. = #.875 RO2-R. + #.125 RO2-N. + RO2. + #.302 HCHO + #.609 CCHO + #.548 RCHO + #.104 ACET + #.079 MEK + #.053 BALD + #.852 -C
O3O3	2.30E-01	2.48E+00	1.42	0.00	OLE3 + O3 = #.24 HCHO + #.269 CCHO + #.373 RCHO + #.056 MEK + #.024 BALD + #.978 -C + #.106 (HCHO2) + #.427 (CCHO2) + #.253 (RCHO2) + #.143 (C(C)CO2 + #.035 (C(R)CO2 + #.036 (BZCHO2)
O3N3	1.53E+03	7.67E+02	-0.41	0.00	OLE3 + NO3 = R2O2. + RO2. + #.346 HCHO + #.696 CCHO + #.626 RCHO + #.119 ACET + #.091 MEK + #.06 BALD + #.883 -C + NO2
O3OA	3.37E+04	1.15E+04	-0.64	0.00	OLE3 + O = #.4 HO2. + #.5 RCHO + #.5 MEK + #2.14 -C + #.4 OLE-RI

[a] Except as noted, expression for rate constant is $k = A\ e^{Ea/RT}\ (T/300)^B$. Rate constants and A factor are in ppm, min units. Units of Ea is kcal $mole^{-1}$. "Phot Set" means this is a photolysis reaction, with the absorption coefficients and quantum yields given in Table A-5.

[b] Format of reaction listing same as used in documentation of the detailed mechanism (Carter 1990).

[c] "#RCONnn" as a reactant means that the rate constant for the reaction is obtained by multiplying the rate constant given by that for reaction "nn". Thus, the rate constant given is actually an equilibrium constant.

[d] Rate constants and product yield parameters based on the mixture of species in the base ROG mixture which are being represented.

[e] Lumping of alkanes with aromatics is not recommended for grid model simulations or for trajectory simulations where the composition of emitted ROG species vary with time. This is not the case with these EKMA simulations.

Table A-3. Absorption cross sections and quantum yields for photolysis reactions.

WL (nm)	Abs (cm^2)	QY	WL (nm)	Abs (cm^2)	QY	WL (nm)	Abs (cm^2)	QY	WL (nm)	Abs (cm^2)	QY	WL (nm)	Abs (cm^2)	QY
Photolysis File = NO2														
250.0	2.83E-20	1.000	255.0	1.45E-20	1.000	260.0	1.90E-20	1.000	265.0	2.05E-20	1.000	270.0	3.13E-20	1.000
275.0	4.02E-20	1.000	280.0	5.54E-20	1.000	285.0	6.99E-20	1.000	290.0	8.18E-20	0.999	295.0	9.67E-20	0.998
300.0	1.17E-19	0.997	305.0	1.66E-19	0.996	310.0	1.76E-19	0.995	315.0	2.25E-19	0.994	320.0	2.54E-19	0.993
325.0	2.79E-19	0.992	330.0	2.99E-19	0.991	335.0	3.45E-19	0.990	340.0	3.88E-19	0.989	345.0	4.07E-19	0.988
350.0	4.10E-19	0.987	355.0	5.13E-19	0.986	360.0	4.51E-19	0.984	365.0	5.78E-19	0.983	370.0	5.42E-19	0.981
375.0	5.35E-19	0.979	380.0	5.99E-19	0.975	381.0	5.98E-19	0.974	382.0	5.97E-19	0.973	383.0	5.96E-19	0.972
384.0	5.95E-19	0.971	385.0	5.94E-19	0.969	386.0	5.95E-19	0.967	387.0	5.96E-19	0.966	388.0	5.98E-19	0.964
389.0	5.99E-19	0.962	390.0	6.00E-19	0.960	391.0	5.98E-19	0.959	392.0	5.96E-19	0.957	393.0	5.93E-19	0.953
394.0	5.91E-19	0.950	395.0	5.89E-19	0.942	396.0	6.06E-19	0.922	397.0	6.24E-19	0.870	398.0	6.41E-19	0.820
399.0	6.59E-19	0.760	400.0	6.76E-19	0.695	401.0	6.67E-19	0.635	402.0	6.58E-19	0.560	403.0	6.50E-19	0.485
404.0	6.41E-19	0.425	405.0	6.32E-19	0.350	406.0	6.21E-19	0.290	407.0	6.10E-19	0.225	408.0	5.99E-19	0.185
409.0	5.88E-19	0.153	410.0	5.77E-19	0.130	411.0	5.88E-19	0.110	412.0	5.98E-19	0.094	413.0	6.09E-19	0.083
414.0	6.19E-19	0.070	415.0	6.30E-19	0.059	416.0	6.29E-19	0.048	417.0	6.27E-19	0.039	418.0	6.26E-19	0.030
419.0	6.24E-19	0.023	420.0	6.23E-19	0.018	421.0	6.18E-19	0.012	422.0	6.14E-19	0.008	423.0	6.09E-19	0.004
424.0	6.05E-19	0.000	425.0	6.00E-19	0.000									
Photolysis File = NO3NO														
585.0	2.77E-18	0.000	590.0	5.14E-18	0.250	595.0	4.08E-18	0.400	600.0	2.83E-18	0.250	605.0	3.45E-18	0.200
610.0	1.48E-18	0.200	615.0	1.96E-18	0.100	620.0	3.58E-18	0.100	625.0	9.25E-18	0.050	630.0	5.66E-18	0.050
635.0	1.45E-18	0.030	640.0	1.11E-18	0.000									
Photolysis File = NO3NO2														
400.0	0.00E+00	1.000	405.0	3.00E-20	1.000	410.0	4.00E-20	1.000	415.0	5.00E-20	1.000	420.0	8.00E-20	1.000
425.0	1.00E-19	1.000	430.0	1.30E-19	1.000	435.0	1.80E-19	1.000	440.0	1.90E-19	1.000	445.0	2.20E-19	1.000
450.0	2.80E-19	1.000	455.0	3.30E-19	1.000	460.0	3.70E-19	1.000	465.0	4.30E-19	1.000	470.0	5.10E-19	1.000
475.0	6.00E-19	1.000	480.0	6.40E-19	1.000	485.0	6.90E-19	1.000	490.0	8.80E-19	1.000	495.0	9.50E-19	1.000
500.0	1.01E-18	1.000	505.0	1.10E-18	1.000	510.0	1.32E-18	1.000	515.0	1.40E-18	1.000	520.0	1.45E-18	1.000
525.0	1.48E-18	1.000	530.0	1.94E-18	1.000	535.0	2.04E-18	1.000	540.0	1.81E-18	1.000	545.0	1.81E-18	1.000
550.0	2.36E-18	1.000	555.0	2.68E-18	1.000	560.0	3.07E-18	1.000	565.0	2.53E-18	1.000	570.0	2.54E-18	1.000
575.0	2.74E-18	1.000	580.0	3.05E-18	1.000	585.0	2.77E-18	1.000	590.0	5.14E-18	0.750	595.0	4.08E-18	0.600
600.0	2.83E-18	0.550	605.0	3.45E-18	0.400	610.0	1.45E-18	0.300	615.0	1.96E-18	0.250	620.0	3.58E-18	0.200
625.0	9.25E-18	0.150	630.0	5.66E-18	0.050	635.0	1.45E-18	0.000						
Photolysis File = O3O3P														
280.0	3.97E-18	0.100	281.0	3.60E-18	0.100	282.0	3.24E-18	0.100	283.0	3.01E-18	0.100	284.0	2.73E-18	0.100
285.0	2.44E-18	0.100	286.0	2.21E-18	0.100	287.0	2.01E-18	0.100	288.0	1.76E-18	0.100	289.0	1.58E-18	0.100
290.0	1.41E-18	0.100	291.0	1.26E-18	0.100	292.0	1.10E-18	0.100	293.0	9.89E-19	0.100	294.0	8.59E-19	0.100
295.0	7.70E-19	0.100	296.0	6.67E-19	0.100	297.0	5.84E-19	0.100	298.0	5.07E-19	0.100	299.0	4.52E-19	0.100
300.0	3.92E-19	0.100	301.0	3.42E-19	0.100	302.0	3.06E-19	0.100	303.0	2.60E-19	0.100	304.0	2.37E-19	0.100
305.0	2.01E-19	0.112	306.0	1.79E-19	0.149	307.0	1.56E-19	0.197	308.0	1.38E-19	0.259	309.0	1.25E-19	0.339
310.0	1.02E-19	0.437	311.0	9.17E-20	0.546	312.0	7.88E-20	0.652	313.0	6.77E-20	0.743	314.0	6.35E-20	0.816
315.0	5.10E-20	0.872	316.0	4.61E-20	0.916	317.0	4.17E-20	0.949	318.0	3.72E-20	0.976	319.0	2.69E-20	0.997
320.0	3.23E-20	1.000	330.0	6.70E-21	1.000	340.0	1.70E-21	1.000	350.0	4.00E-22	1.000	355.0	0.00E+00	1.000
400.0	0.00E+00	1.000	450.0	1.60E-22	1.000	500.0	1.34E-21	1.000	550.0	3.32E-21	1.000	600.0	5.06E-21	1.000
650.0	2.45E-21	1.000	700.0	8.70E-22	1.000	750.0	3.20E-22	1.000	800.0	1.60E-22	1.000	900.0	0.00E+00	1.000
Photolysis File = O3O1D														
280.0	3.97E-18	0.900	281.0	3.60E-18	0.900	282.0	3.24E-18	0.900	283.0	3.01E-18	0.900	284.0	2.73E-18	0.900
285.0	2.44E-18	0.900	286.0	2.21E-18	0.900	287.0	2.01E-18	0.900	288.0	1.76E-18	0.900	289.0	1.58E-18	0.900
290.0	1.41E-18	0.900	291.0	1.26E-18	0.900	292.0	1.10E-18	0.900	293.0	9.89E-19	0.900	294.0	8.59E-19	0.900
295.0	7.70E-19	0.900	296.0	6.67E-19	0.900	297.0	5.84E-19	0.900	298.0	5.07E-19	0.900	299.0	4.52E-19	0.900
300.0	3.92E-19	0.900	301.0	3.42E-19	0.900	302.0	3.06E-19	0.900	303.0	2.60E-19	0.900	304.0	2.37E-19	0.900
305.0	2.01E-19	0.888	306.0	1.79E-19	0.851	307.0	1.56E-19	0.803	308.0	1.38E-19	0.741	309.0	1.25E-19	0.661
310.0	1.02E-19	0.563	311.0	9.17E-20	0.454	312.0	7.88E-20	0.348	313.0	6.77E-20	0.257	314.0	6.35E-20	0.184
315.0	5.10E-20	0.128	316.0	4.61E-20	0.084	317.0	4.17E-20	0.051	318.0	3.72E-20	0.024	319.0	2.69E-20	0.003
320.0	3.23E-20	0.000												
Photolysis File = HONO														
311.0	0.00E+00	1.000	312.0	2.00E-21	1.000	313.0	4.20E-21	1.000	314.0	4.60E-21	1.000	315.0	4.20E-21	1.000
316.0	3.00E-21	1.000	317.0	4.60E-21	1.000	318.0	3.60E-20	1.000	319.0	6.10E-20	1.000	320.0	2.10E-20	1.000
321.0	4.27E-20	1.000	322.0	4.01E-20	1.000	323.0	3.93E-20	1.000	324.0	4.01E-20	1.000	325.0	4.04E-20	1.000
326.0	3.13E-20	1.000	327.0	4.12E-20	1.000	328.0	7.55E-20	1.000	329.0	6.64E-20	1.000	330.0	7.29E-20	1.000
331.0	8.70E-20	1.000	332.0	1.38E-19	1.000	333.0	5.91E-20	1.000	334.0	5.91E-20	1.000	335.0	6.45E-20	1.000
336.0	5.91E-20	1.000	337.0	4.58E-20	1.000	338.0	1.91E-19	1.000	339.0	1.63E-19	1.000	340.0	1.05E-19	1.000
341.0	8.70E-20	1.000	342.0	3.35E-19	1.000	343.0	2.01E-19	1.000	344.0	1.02E-19	1.000	345.0	8.54E-20	1.000
346.0	8.32E-20	1.000	347.0	8.20E-20	1.000	348.0	7.49E-20	1.000	349.0	7.13E-20	1.000	350.0	6.83E-20	1.000
351.0	1.74E-19	1.000	352.0	1.14E-19	1.000	353.0	3.71E-19	1.000	354.0	4.96E-19	1.000	355.0	2.46E-19	1.000
356.0	1.19E-19	1.000	357.0	9.35E-20	1.000	358.0	7.78E-20	1.000	359.0	7.29E-20	1.000	360.0	6.83E-20	1.000
361.0	6.90E-20	1.000	362.0	7.32E-20	1.000	363.0	9.00E-20	1.000	364.0	1.21E-19	1.000	365.0	1.33E-19	1.000
366.0	2.13E-19	1.000	367.0	3.52E-19	1.000	368.0	4.50E-19	1.000	369.0	2.93E-19	1.000	370.0	1.19E-19	1.000
371.0	9.46E-20	1.000	372.0	8.85E-20	1.000	373.0	7.44E-20	1.000	374.0	4.77E-20	1.000	375.0	2.70E-20	1.000
376.0	1.90E-20	1.000	377.0	1.50E-20	1.000	378.0	1.90E-20	1.000	379.0	5.80E-20	1.000	380.0	7.78E-20	1.000
381.0	1.14E-19	1.000	382.0	1.40E-19	1.000	383.0	1.72E-19	1.000	384.0	1.99E-19	1.000	385.0	1.90E-19	1.000
386.0	1.19E-19	1.000	387.0	5.65E-20	1.000	388.0	3.20E-20	1.000	389.0	1.90E-20	1.000	390.0	1.20E-20	1.000
391.0	5.00E-21	1.000	392.0	0.00E+00	1.000									
Photolysis File = H2O2														
250.0	8.30E-20	1.000	255.0	6.70E-20	1.000	260.0	5.20E-20	1.000	265.0	4.20E-20	1.000	270.0	3.20E-20	1.000
275.0	2.50E-20	1.000	280.0	2.00E-20	1.000	285.0	1.50E-20	1.000	290.0	1.13E-20	1.000	295.0	8.70E-21	1.000
300.0	6.60E-21	1.000	305.0	4.90E-21	1.000	310.0	3.70E-21	1.000	315.0	2.80E-21	1.000	320.0	2.00E-21	1.000
325.0	1.50E-21	1.000	330.0	1.20E-21	1.000	335.0	9.00E-22	1.000	340.0	7.00E-22	1.000	345.0	5.00E-22	1.000
350.0	3.00E-22	1.000	355.0	0.00E+00	1.000									

Table A-3. (continued)

WL (nm)	Abs (cm^2)	QY	WL (nm)	Abs (cm^2)	QY	WL (nm)	Abs (cm^2)	QY	WL (nm)	Abs (cm^2)	QY	WL (nm)	Abs (cm^2)	QY
Photolysis File = HCHONEWR														
280.0	2.49E-20	0.590	280.5	1.42E-20	0.596	281.0	1.51E-20	0.602	281.5	1.32E-20	0.608	282.0	9.73E-21	0.614
282.5	6.76E-21	0.620	283.0	5.82E-21	0.626	283.5	9.10E-21	0.632	284.0	3.71E-20	0.638	284.5	4.81E-20	0.644
285.0	3.95E-20	0.650	285.5	2.87E-20	0.656	286.0	2.24E-20	0.662	286.5	1.74E-20	0.668	287.0	1.13E-20	0.674
287.5	1.10E-20	0.680	288.0	2.62E-20	0.686	288.5	4.00E-20	0.692	289.0	3.55E-20	0.698	289.5	2.12E-20	0.704
290.0	1.07E-20	0.710	290.5	1.35E-20	0.713	291.0	1.99E-20	0.717	291.5	1.56E-20	0.721	292.0	8.65E-21	0.724
292.5	5.90E-21	0.727	293.0	1.11E-20	0.731	293.5	6.26E-20	0.735	294.0	7.40E-20	0.738	294.5	5.36E-20	0.741
295.0	4.17E-20	0.745	295.5	3.51E-20	0.749	296.0	2.70E-20	0.752	296.5	1.75E-20	0.755	297.0	1.16E-20	0.759
297.5	1.51E-20	0.763	298.0	3.69E-20	0.766	298.5	4.40E-20	0.769	299.0	3.44E-20	0.773	299.5	2.02E-20	0.776
300.0	1.06E-20	0.780	300.4	7.01E-21	0.780	300.6	8.63E-21	0.779	300.8	1.47E-20	0.779	301.0	2.01E-20	0.779
301.2	2.17E-20	0.779	301.4	1.96E-20	0.779	301.6	1.54E-20	0.778	301.8	1.26E-20	0.778	302.0	1.03E-20	0.778
302.2	8.53E-21	0.778	302.4	7.13E-21	0.778	302.6	6.61E-21	0.777	302.8	1.44E-20	0.777	303.0	3.18E-20	0.777
303.2	3.81E-20	0.777	303.4	5.57E-20	0.777	303.6	6.91E-20	0.776	303.8	6.58E-20	0.776	304.0	6.96E-20	0.776
304.2	5.79E-20	0.776	304.4	5.24E-20	0.776	304.6	4.30E-20	0.775	304.8	3.28E-20	0.775	305.0	3.60E-20	0.775
305.2	5.12E-20	0.775	305.4	4.77E-20	0.775	305.6	4.43E-20	0.774	305.8	4.60E-20	0.774	306.0	4.01E-20	0.774
306.2	3.28E-20	0.774	306.4	2.66E-20	0.774	306.6	2.42E-20	0.773	306.8	1.95E-20	0.773	307.0	1.58E-20	0.773
307.2	1.37E-20	0.773	307.4	1.19E-20	0.773	307.6	1.01E-20	0.772	307.8	9.01E-21	0.772	308.0	8.84E-21	0.772
308.2	2.08E-20	0.772	308.4	2.39E-20	0.772	308.6	3.08E-20	0.771	308.8	3.39E-20	0.771	309.0	3.18E-20	0.771
309.2	3.06E-20	0.771	309.4	2.84E-20	0.771	309.6	2.46E-20	0.770	309.8	1.95E-20	0.770	310.0	1.57E-20	0.770
310.2	1.26E-20	0.767	310.4	9.26E-21	0.764	310.6	7.71E-21	0.761	310.8	6.05E-21	0.758	311.0	5.13E-21	0.755
311.2	4.82E-21	0.752	311.4	4.54E-21	0.749	311.6	6.81E-21	0.746	311.8	1.04E-20	0.743	312.0	1.43E-20	0.740
312.2	1.47E-20	0.737	312.4	1.35E-20	0.734	312.6	1.13E-20	0.731	312.8	9.86E-21	0.728	313.0	7.82E-21	0.725
313.2	6.48E-21	0.722	313.4	1.07E-20	0.719	313.6	2.39E-20	0.716	313.8	3.80E-20	0.713	314.0	5.76E-20	0.710
314.2	6.14E-20	0.707	314.4	7.45E-20	0.704	314.6	5.78E-20	0.701	314.8	5.59E-20	0.698	315.0	4.91E-20	0.695
315.2	4.37E-20	0.692	315.4	3.92E-20	0.689	315.6	2.89E-20	0.686	315.8	2.82E-20	0.683	316.0	2.10E-20	0.680
316.2	1.66E-20	0.677	316.4	2.05E-20	0.674	316.6	4.38E-20	0.671	316.8	5.86E-20	0.668	317.0	6.28E-20	0.665
317.2	5.07E-20	0.662	317.4	4.33E-20	0.659	317.6	4.17E-20	0.656	317.8	3.11E-20	0.653	318.0	2.64E-20	0.650
318.2	2.24E-20	0.647	318.4	1.70E-20	0.644	318.6	1.24E-20	0.641	318.8	1.11E-20	0.638	319.0	7.70E-21	0.635
319.2	6.36E-21	0.632	319.4	5.36E-21	0.629	319.6	4.79E-21	0.626	319.8	6.48E-21	0.623	320.0	1.48E-20	0.620
320.2	1.47E-20	0.614	320.4	1.36E-20	0.608	320.6	1.69E-20	0.601	320.8	1.32E-20	0.595	321.0	1.49E-20	0.589
321.2	1.17E-20	0.583	321.4	1.15E-20	0.577	321.6	9.64E-21	0.570	321.8	7.26E-21	0.564	322.0	5.94E-21	0.558
322.2	4.13E-21	0.552	322.4	3.36E-21	0.546	322.6	2.39E-21	0.539	322.8	2.01E-21	0.533	323.0	1.76E-21	0.527
323.2	2.82E-21	0.521	323.4	4.65E-21	0.515	323.6	7.00E-21	0.508	323.8	7.80E-21	0.502	324.0	7.87E-21	0.496
324.2	6.59E-21	0.490	324.4	5.60E-21	0.484	324.6	4.66E-21	0.477	324.8	4.21E-21	0.471	325.0	7.77E-21	0.465
325.2	2.15E-20	0.459	325.4	3.75E-20	0.453	325.6	4.10E-20	0.446	325.8	6.47E-20	0.440	326.0	7.59E-20	0.434
326.2	6.51E-20	0.428	326.4	5.53E-20	0.422	326.6	5.76E-20	0.415	326.8	4.43E-20	0.409	327.0	3.44E-20	0.403
327.2	3.22E-20	0.397	327.4	2.13E-20	0.391	327.6	1.91E-20	0.384	327.8	1.42E-20	0.378	328.0	9.15E-21	0.372
328.2	6.79E-21	0.366	328.4	4.99E-21	0.360	328.6	4.77E-21	0.353	328.8	1.75E-20	0.347	329.0	3.27E-20	0.341
329.2	3.99E-20	0.335	329.4	5.13E-20	0.329	329.6	4.00E-20	0.322	329.8	3.61E-20	0.316	330.0	3.38E-20	0.310
330.2	3.08E-20	0.304	330.4	2.16E-20	0.298	330.6	2.09E-20	0.291	330.8	1.41E-20	0.285	331.0	9.95E-21	0.279
331.2	7.76E-21	0.273	331.4	6.16E-21	0.267	331.6	4.06E-21	0.260	331.8	3.03E-21	0.254	332.0	2.41E-21	0.248
332.2	1.74E-21	0.242	332.4	1.33E-21	0.236	332.6	2.70E-21	0.229	332.8	1.65E-21	0.223	333.0	1.17E-21	0.217
333.2	9.84E-22	0.211	333.4	8.52E-22	0.205	333.6	6.32E-22	0.198	333.8	5.21E-22	0.192	334.0	1.46E-21	0.186
334.2	1.80E-21	0.180	334.4	1.43E-21	0.174	334.6	1.03E-21	0.167	334.8	7.19E-22	0.161	335.0	4.84E-22	0.155
335.2	2.73E-22	0.149	335.4	1.34E-22	0.143	335.6	-1.62E-22	0.136	335.8	1.25E-22	0.130	336.0	4.47E-22	0.124
336.2	1.23E-21	0.118	336.4	2.02E-21	0.112	336.6	3.00E-21	0.105	336.8	2.40E-21	0.099	337.0	3.07E-21	0.093
337.2	2.29E-21	0.087	337.4	2.46E-21	0.081	337.6	2.92E-21	0.074	337.8	8.10E-21	0.068	338.0	1.82E-20	0.062
338.2	3.10E-20	0.056	338.4	3.24E-20	0.050	338.6	4.79E-20	0.043	338.8	5.25E-20	0.037	339.0	5.85E-20	0.031
339.2	4.33E-20	0.025	339.4	4.20E-20	0.019	339.6	3.99E-20	0.012	339.8	3.11E-20	0.006	340.0	2.72E-20	0.000
Photolysis File = HCHONEWM														
280.0	2.49E-20	0.350	280.5	1.42E-20	0.346	281.0	1.51E-20	0.341	281.5	1.32E-20	0.336	282.0	9.73E-21	0.332
282.5	6.76E-21	0.327	283.0	5.82E-21	0.323	283.5	9.10E-21	0.319	284.0	3.71E-20	0.314	284.5	4.81E-20	0.309
285.0	3.95E-20	0.305	285.5	2.87E-20	0.301	286.0	2.24E-20	0.296	286.5	1.74E-20	0.291	287.0	1.13E-20	0.287
287.5	1.10E-20	0.282	288.0	2.62E-20	0.278	288.5	4.00E-20	0.273	289.0	3.55E-20	0.269	289.5	2.12E-20	0.264
290.0	1.07E-20	0.260	290.5	1.35E-20	0.258	291.0	1.99E-20	0.256	291.5	1.56E-20	0.254	292.0	8.65E-21	0.252
292.5	5.90E-21	0.250	293.0	1.11E-20	0.248	293.5	6.26E-20	0.246	294.0	7.40E-20	0.244	294.5	5.36E-20	0.242
295.0	4.17E-20	0.240	295.5	3.51E-20	0.238	296.0	2.70E-20	0.236	296.5	1.75E-20	0.234	297.0	1.16E-20	0.232
297.5	1.51E-20	0.230	298.0	3.69E-20	0.228	298.5	4.40E-20	0.226	299.0	3.44E-20	0.224	299.5	2.02E-20	0.222
300.0	1.06E-20	0.220	300.4	7.01E-21	0.220	300.6	8.63E-21	0.221	300.8	1.47E-20	0.221	301.0	2.01E-20	0.221
301.2	2.17E-20	0.221	301.4	1.96E-20	0.221	301.6	1.54E-20	0.222	301.8	1.26E-20	0.222	302.0	1.03E-20	0.222
302.2	8.53E-21	0.222	302.4	7.13E-21	0.222	302.6	6.61E-21	0.223	302.8	1.44E-20	0.223	303.0	3.18E-20	0.223
303.2	3.81E-20	0.223	303.4	5.57E-20	0.223	303.6	6.91E-20	0.224	303.8	6.58E-20	0.224	304.0	6.96E-20	0.224
304.2	5.79E-20	0.224	304.4	5.24E-20	0.224	304.6	4.30E-20	0.225	304.8	3.28E-20	0.225	305.0	3.60E-20	0.225
305.2	5.12E-20	0.225	305.4	4.77E-20	0.225	305.6	4.43E-20	0.226	305.8	4.60E-20	0.226	306.0	4.01E-20	0.226
306.2	3.28E-20	0.226	306.4	2.66E-20	0.226	306.6	2.42E-20	0.227	306.8	1.95E-20	0.227	307.0	1.58E-20	0.227
307.2	1.37E-20	0.227	307.4	1.19E-20	0.227	307.6	1.01E-20	0.228	307.8	9.01E-21	0.228	308.0	8.84E-21	0.228
308.2	2.08E-20	0.228	308.4	2.39E-20	0.228	308.6	3.08E-20	0.229	308.8	3.39E-20	0.229	309.0	3.18E-20	0.229
309.2	3.06E-20	0.229	309.4	2.84E-20	0.229	309.6	2.46E-20	0.230	309.8	1.95E-20	0.230	310.0	1.57E-20	0.230
310.2	1.26E-20	0.233	310.4	9.26E-21	0.236	310.6	7.71E-21	0.239	310.8	6.05E-21	0.242	311.0	5.13E-21	0.245
311.2	4.82E-21	0.248	311.4	4.54E-21	0.251	311.6	6.81E-21	0.254	311.8	1.04E-20	0.257	312.0	1.43E-20	0.260
312.2	1.47E-20	0.263	312.4	1.35E-20	0.266	312.6	1.13E-20	0.269	312.8	9.86E-21	0.272	313.0	7.82E-21	0.275
313.2	6.48E-21	0.278	313.4	1.07E-20	0.281	313.6	2.39E-20	0.284	313.8	3.80E-20	0.287	314.0	5.76E-20	0.290
314.2	6.14E-20	0.293	314.4	7.45E-20	0.296	314.6	5.78E-20	0.299	314.8	5.59E-20	0.302	315.0	4.91E-20	0.305
315.2	4.37E-20	0.308	315.4	3.92E-20	0.311	315.6	2.89E-20	0.314	315.8	2.82E-20	0.317	316.0	2.10E-20	0.320
316.2	1.66E-20	0.323	316.4	2.05E-20	0.326	316.6	4.38E-20	0.329	316.8	5.86E-20	0.332	317.0	6.28E-20	0.335
317.2	5.07E-20	0.338	317.4	4.33E-20	0.341	317.6	4.17E-20	0.344	317.8	3.11E-20	0.347	318.0	2.64E-20	0.350
318.2	2.24E-20	0.353	318.4	1.70E-20	0.356	318.6	1.24E-20	0.359	318.8	1.11E-20	0.362	319.0	7.70E-21	0.365
319.2	6.36E-21	0.368	319.4	5.36E-21	0.371	319.6	4.79E-21	0.374	319.8	6.48E-21	0.377	320.0	1.48E-20	0.380
320.2	1.47E-20	0.386	320.4	1.36E-20	0.392	320.6	1.69E-20	0.399	320.8	1.32E-20	0.405	321.0	1.49E-20	0.411
321.2	1.17E-20	0.417	321.4	1.15E-20	0.423	321.6	9.64E-21	0.430	321.8	7.26E-21	0.436	322.0	5.94E-21	0.442
322.2	4.13E-21	0.448	322.4	3.36E-21	0.454	322.6	2.39E-21	0.461	322.8	2.01E-21	0.467	323.0	1.76E-21	0.473
323.2	2.82E-21	0.479	323.4	4.65E-21	0.485	323.6	7.00E-21	0.492	323.8	7.80E-21	0.498	324.0	7.87E-21	0.504
324.2	6.59E-21	0.510	324.4	5.60E-21	0.516	324.6	4.66E-21	0.523	324.8	4.21E-21	0.529	325.0	7.77E-21	0.535

Table A-3. (continued)

WL (nm)	Abs (cm^2)	QY	WL (nm)	Abs (cm^2)	QY	WL (nm)	Abs (cm^2)	QY	WL (nm)	Abs (cm^2)	QY	WL (nm)	Abs (cm^2)	QY
325.2	2.15E-20	0.541	325.4	3.75E-20	0.547	325.6	4.10E-20	0.554	325.8	6.47E-20	0.560	326.0	7.59E-20	0.566
326.2	6.51E-20	0.572	326.4	5.53E-20	0.578	326.6	5.76E-20	0.585	326.8	4.43E-20	0.591	327.0	3.44E-20	0.597
327.2	3.22E-20	0.603	327.4	2.13E-20	0.609	327.6	1.91E-20	0.616	327.8	1.42E-20	0.622	328.0	9.15E-21	0.628
328.2	6.79E-21	0.634	328.4	4.99E-21	0.640	328.6	4.77E-21	0.647	328.8	1.75E-20	0.653	329.0	3.27E-20	0.659
329.2	3.99E-20	0.665	329.4	5.13E-20	0.671	329.6	4.00E-20	0.678	329.8	3.61E-20	0.684	330.0	3.38E-20	0.690
330.2	3.08E-20	0.694	330.4	2.16E-20	0.699	330.6	2.09E-20	0.703	330.8	1.41E-20	0.708	331.0	9.95E-21	0.712
331.2	7.76E-21	0.717	331.4	6.16E-21	0.721	331.6	4.06E-21	0.726	331.8	3.03E-21	0.730	332.0	2.41E-21	0.735
332.2	1.74E-21	0.739	332.4	1.33E-21	0.744	332.6	2.70E-21	0.748	332.8	1.65E-21	0.753	333.0	1.17E-21	0.757
333.2	9.84E-22	0.762	333.4	8.52E-22	0.766	333.6	6.32E-22	0.771	333.8	5.21E-22	0.775	334.0	1.46E-21	0.780
334.2	1.80E-21	0.784	334.4	1.43E-21	0.789	334.6	1.03E-21	0.793	334.8	7.19E-22	0.798	335.0	4.84E-22	0.802
335.2	2.73E-22	0.798	335.4	1.34E-22	0.794	335.6	0.00E+00	0.790	335.8	1.25E-22	0.786	336.0	4.47E-22	0.782
336.2	1.23E-21	0.778	336.4	2.02E-21	0.773	336.6	3.00E-21	0.769	336.8	2.40E-21	0.764	337.0	3.07E-21	0.759
337.2	2.29E-21	0.754	337.4	2.46E-21	0.749	337.6	2.92E-21	0.745	337.8	8.10E-21	0.740	338.0	1.82E-20	0.734
338.2	3.10E-20	0.729	338.4	3.24E-20	0.724	338.6	4.79E-20	0.719	338.8	5.25E-20	0.714	339.0	5.85E-20	0.709
339.2	4.33E-20	0.703	339.4	4.20E-20	0.698	339.6	3.99E-20	0.693	339.8	3.11E-20	0.687	340.0	2.72E-20	0.682
340.2	1.99E-20	0.676	340.4	1.76E-20	0.671	340.6	1.39E-20	0.666	340.8	1.01E-20	0.660	341.0	6.57E-21	0.655
341.2	4.83E-21	0.649	341.4	3.47E-21	0.643	341.6	2.23E-21	0.638	341.8	1.55E-21	0.632	342.0	3.70E-21	0.627
342.2	4.64E-21	0.621	342.4	1.08E-20	0.616	342.6	1.14E-20	0.610	342.8	1.79E-20	0.604	343.0	2.33E-20	0.599
343.2	1.72E-20	0.593	343.4	1.55E-20	0.588	343.6	1.46E-20	0.582	343.8	1.38E-20	0.576	344.0	1.00E-20	0.571
344.2	8.26E-21	0.565	344.4	6.32E-21	0.559	344.6	4.28E-21	0.554	344.8	3.22E-21	0.548	345.0	2.54E-21	0.542
345.2	1.60E-21	0.537	345.4	1.15E-21	0.531	345.6	8.90E-22	0.525	345.8	6.50E-22	0.520	346.0	5.09E-22	0.514
346.2	5.15E-22	0.508	346.4	3.45E-22	0.503	346.6	3.18E-22	0.497	346.8	3.56E-22	0.491	347.0	3.24E-22	0.485
347.2	3.34E-22	0.480	347.4	2.88E-22	0.474	347.6	2.84E-22	0.468	347.8	9.37E-22	0.463	348.0	9.70E-22	0.457
348.2	7.60E-22	0.451	348.4	6.24E-22	0.446	348.6	4.99E-22	0.440	348.8	4.08E-22	0.434	349.0	3.39E-22	0.428
349.2	1.64E-22	0.423	349.4	1.49E-22	0.417	349.6	8.30E-23	0.411	349.8	2.52E-23	0.406	350.0	2.57E-23	0.400
350.2	0.00E+00	0.394	350.4	5.16E-23	0.389	350.6	0.00E+00	0.383	350.8	2.16E-23	0.377	351.0	7.07E-23	0.371
351.2	3.45E-23	0.366	351.4	1.97E-22	0.360	351.6	4.80E-22	0.354	351.8	3.13E-21	0.349	352.0	6.41E-21	0.343
352.2	8.38E-21	0.337	352.4	1.55E-20	0.331	352.6	1.86E-20	0.326	352.8	1.94E-20	0.320	353.0	2.78E-20	0.314
353.2	1.96E-20	0.309	353.4	1.67E-20	0.303	353.6	1.75E-20	0.297	353.8	1.63E-20	0.291	354.0	1.36E-20	0.286
354.2	1.07E-20	0.280	354.4	9.82E-21	0.274	354.6	8.66E-21	0.269	354.8	6.44E-21	0.263	355.0	4.84E-21	0.257
355.2	3.49E-21	0.251	355.4	2.41E-21	0.246	355.6	1.74E-21	0.240	355.8	1.11E-21	0.234	356.0	7.37E-22	0.229
356.2	4.17E-22	0.223	356.4	1.95E-22	0.217	356.6	1.50E-22	0.211	356.8	8.14E-23	0.206	357.0	0.00E+00	0.200
Photolysis File = CCHOR														
260.0	2.00E-20	0.310	270.0	3.40E-20	0.390	280.0	4.50E-20	0.580	290.0	4.90E-20	0.530	295.0	4.50E-20	0.480
300.0	4.30E-20	0.430	305.0	3.40E-20	0.370	315.0	2.10E-20	0.170	320.0	1.80E-20	0.100	325.0	1.10E-20	0.040
330.0	6.90E-21	0.000												
Photolysis File = RCHO														
280.0	5.26E-20	0.960	290.0	5.77E-20	0.910	300.0	5.05E-20	0.860	310.0	3.68E-20	0.600	320.0	1.66E-20	0.360
330.0	6.49E-21	0.200	340.0	1.44E-21	0.080	345.0	0.00E+00	0.020						
Photolysis File = ACET-93C (Standard Mechanism)														
250.0	2.37E-20	0.760	260.0	3.66E-20	0.800	270.0	4.63E-20	0.640	280.0	5.05E-20	0.550	290.0	4.21E-20	0.300
300.0	2.78E-20	0.150	310.0	1.44E-20	0.050	320.0	4.80E-21	0.026	330.0	8.00E-22	0.017	340.0	1.00E-22	0.000
350.0	3.00E-23	0.000	360.0	0.00E+00	0.000									
Photolysis File = ADJACET (Adjusted Mechanism)														
250.0	2.37E-20	0.760	260.0	3.66E-20	0.800	270.0	4.63E-20	0.640	280.0	5.05E-20	0.600	290.0	4.21E-20	0.600
300.0	2.78E-20	0.300	310.0	1.44E-20	0.005	320.0	4.80E-21	0.000	330.0	8.00E-22	0.000	340.0	1.00E-22	0.000
350.0	3.00E-23	0.000	360.0	0.00E+00	0.000									
Photolysis File = KETONE														
210.0	1.10E-21	0.100	220.0	1.20E-21	0.100	230.0	4.60E-21	0.100	240.0	1.30E-20	0.100	250.0	2.68E-20	0.100
260.0	4.21E-20	0.100	270.0	5.54E-20	0.100	280.0	5.92E-20	0.100	290.0	5.16E-20	0.100	300.0	3.44E-20	0.100
310.0	1.53E-20	0.100	320.0	4.60E-21	0.100	330.0	1.10E-21	0.100	340.0	0.00E+00	0.100			
Photolysis File = CO2H														
210.0	3.75E-19	1.000	220.0	2.20E-19	1.000	230.0	1.38E-19	1.000	240.0	8.80E-20	1.000	250.0	5.80E-20	1.000
260.0	3.80E-20	1.000	270.0	2.50E-20	1.000	280.0	1.50E-20	1.000	290.0	9.00E-21	1.000	300.0	5.80E-21	1.000
310.0	3.40E-21	1.000	320.0	1.90E-21	1.000	330.0	1.10E-21	1.000	340.0	6.00E-22	1.000	350.0	4.00E-22	1.000
360.0	0.00E+00	1.000												
Photolysis File = GLYOXAL1														
230.0	2.87E-21	1.000	235.0	2.87E-21	1.000	240.0	4.30E-21	1.000	245.0	5.73E-21	1.000	250.0	8.60E-21	1.000
255.0	1.15E-20	1.000	260.0	1.43E-20	1.000	265.0	1.86E-20	1.000	270.0	2.29E-20	1.000	275.0	2.58E-20	1.000
280.0	2.87E-20	1.000	285.0	3.30E-20	1.000	290.0	3.15E-20	1.000	295.0	3.30E-20	1.000	300.0	3.58E-20	1.000
305.0	2.72E-20	1.000	310.0	2.72E-20	1.000	312.5	2.87E-20	1.000	315.0	2.29E-20	1.000	320.0	1.43E-20	1.000
325.0	1.15E-20	1.000	327.5	1.43E-20	1.000	330.0	1.15E-20	1.000	335.0	2.87E-21	1.000	340.0	0.00E+00	1.000
Photolysis File = GLYOXAL2														
355.0	0.00E+00	0.029	360.0	2.29E-21	0.029	365.0	2.87E-21	0.029	370.0	8.03E-21	0.029	375.0	1.00E-20	0.029
380.0	1.72E-20	0.029	382.0	1.58E-20	0.029	384.0	1.49E-20	0.029	386.0	1.49E-20	0.029	388.0	2.87E-20	0.029
390.0	3.15E-20	0.029	391.0	3.24E-20	0.029	392.0	3.04E-20	0.029	393.0	2.23E-20	0.029	394.0	2.63E-20	0.029
395.0	3.04E-20	0.029	396.0	2.63E-20	0.029	397.0	2.43E-20	0.029	398.0	3.24E-20	0.029	399.0	3.04E-20	0.029
400.0	2.84E-20	0.029	401.0	3.24E-20	0.029	402.0	4.46E-20	0.029	403.0	5.27E-20	0.029	404.0	4.26E-20	0.029
405.0	3.04E-20	0.029	406.0	3.04E-20	0.029	407.0	2.84E-20	0.029	408.0	2.43E-20	0.029	409.0	2.84E-20	0.029
410.0	6.08E-20	0.029	411.0	5.07E-20	0.029	411.5	6.08E-20	0.029	412.0	4.86E-20	0.029	413.0	8.31E-20	0.029
413.5	6.48E-20	0.029	414.0	7.50E-20	0.029	414.5	8.11E-20	0.029	415.0	8.11E-20	0.029	415.5	6.89E-20	0.029
416.0	4.26E-20	0.029	417.0	4.86E-20	0.029	418.0	5.88E-20	0.029	419.0	6.69E-20	0.029	420.0	3.85E-20	0.029
421.0	5.67E-20	0.029	421.5	4.46E-20	0.029	422.0	5.27E-20	0.029	422.5	1.05E-19	0.029	423.0	8.51E-20	0.029
424.0	6.08E-20	0.029	425.0	7.29E-20	0.029	426.0	1.18E-19	0.029	426.5	1.30E-19	0.029	427.0	1.07E-19	0.029
428.0	1.66E-19	0.029	429.0	4.05E-20	0.029	430.0	5.07E-20	0.029	431.0	4.86E-20	0.029	432.0	4.05E-20	0.029
433.0	3.65E-20	0.029	434.0	4.05E-20	0.029	434.5	6.08E-20	0.029	435.0	5.07E-20	0.029	436.0	8.11E-20	0.029

Table A-3. (continued)

WL (nm)	Abs (cm^2)	QY	WL (nm)	Abs (cm^2)	QY	WL (nm)	Abs (cm^2)	QY	WL (nm)	Abs (cm^2)	QY	WL (nm)	Abs (cm^2)	QY
436.5	1.13E-19	0.029	437.0	5.27E-20	0.029	438.0	1.01E-19	0.029	438.5	1.38E-19	0.029	439.0	7.70E-20	0.029
440.0	2.47E-19	0.029	441.0	8.11E-20	0.029	442.0	6.08E-20	0.029	443.0	7.50E-20	0.029	444.0	9.32E-20	0.029
445.0	1.13E-19	0.029	446.0	5.27E-20	0.029	447.0	2.43E-20	0.029	448.0	2.84E-20	0.029	449.0	3.85E-20	0.029
450.0	6.08E-20	0.029	451.0	1.09E-19	0.029	451.5	9.32E-20	0.029	452.0	1.22E-19	0.029	453.0	2.39E-19	0.029
454.0	1.70E-19	0.029	455.0	3.40E-19	0.029	455.5	4.05E-19	0.029	456.0	1.01E-19	0.029	457.0	1.62E-20	0.029
458.0	1.22E-20	0.029	458.5	1.42E-20	0.029	459.0	4.05E-21	0.029	460.0	4.05E-21	0.029	460.5	6.08E-21	0.029
461.0	2.03E-21	0.029	462.0	0.00E+00	0.029									
Photolysis File = MEGLYOX1														
220.0	2.10E-21	1.000	225.0	2.10E-21	1.000	230.0	4.21E-21	1.000	235.0	7.57E-21	1.000	240.0	9.25E-21	1.000
245.0	8.41E-21	1.000	250.0	9.25E-21	1.000	255.0	9.25E-21	1.000	260.0	9.67E-21	1.000	265.0	1.05E-20	1.000
270.0	1.26E-20	1.000	275.0	1.43E-20	1.000	280.0	1.51E-20	1.000	285.0	1.43E-20	1.000	290.0	1.47E-20	1.000
295.0	1.18E-20	1.000	300.0	1.14E-20	1.000	305.0	9.25E-21	1.000	310.0	6.31E-21	1.000	315.0	5.47E-21	1.000
320.0	3.36E-21	1.000	325.0	1.68E-21	1.000	330.0	8.41E-22	1.000	335.0	0.00E+00	1.000			
Photolysis File = MEGLYOX2														
350.0	0.00E+00	1.000	354.0	4.21E-22	1.000	358.0	1.26E-21	1.000	360.0	2.10E-21	1.000	362.0	2.10E-21	1.000
364.0	2.94E-21	1.000	366.0	3.36E-21	1.000	368.0	4.21E-21	1.000	370.0	5.47E-21	1.000	372.0	5.89E-21	1.000
374.0	7.57E-21	1.000	376.0	7.99E-21	1.000	378.0	8.83E-21	1.000	380.0	1.01E-20	1.000	382.0	1.09E-20	1.000
384.0	1.35E-20	1.000	386.0	1.51E-20	1.000	388.0	1.72E-20	1.000	390.0	2.06E-20	1.000	392.0	2.10E-20	1.000
394.0	2.31E-20	1.000	396.0	2.48E-20	1.000	398.0	2.61E-20	1.000	400.0	2.78E-20	1.000	402.0	2.99E-20	1.000
404.0	3.20E-20	1.000	406.0	3.79E-20	1.000	408.0	3.95E-20	1.000	410.0	4.33E-20	1.000	412.0	4.71E-20	1.000
414.0	4.79E-20	1.000	416.0	4.88E-20	1.000	418.0	5.05E-20	1.000	420.0	5.21E-20	1.000	422.0	5.30E-20	1.000
424.0	5.17E-20	1.000	426.0	5.30E-20	1.000	428.0	5.21E-20	1.000	430.0	5.55E-20	1.000	432.0	5.13E-20	1.000
434.0	5.68E-20	1.000	436.0	6.22E-20	1.000	438.0	6.06E-20	1.000	440.0	5.47E-20	1.000	441.0	6.14E-20	1.000
442.0	5.47E-20	1.000	443.0	5.55E-20	1.000	443.5	6.81E-20	1.000	444.0	5.97E-20	1.000	445.0	5.13E-20	1.000
446.0	4.88E-20	1.000	447.0	5.72E-20	1.000	448.0	5.47E-20	1.000	449.0	6.56E-20	1.000	450.0	5.05E-20	1.000
451.0	3.03E-20	1.000	452.0	4.29E-20	1.000	453.0	2.78E-20	1.000	454.0	2.27E-20	1.000	456.0	1.77E-20	1.000
458.0	8.41E-21	1.000	460.0	4.21E-21	1.000	464.0	1.68E-21	1.000	468.0	0.00E+00	1.000			
Photolysis File = BZCHO														
299.0	1.78E-19	0.050	304.0	7.40E-20	0.050	306.0	6.91E-20	0.050	309.0	6.41E-20	0.050	313.0	6.91E-20	0.050
314.0	6.91E-20	0.050	318.0	6.41E-20	0.050	325.0	8.39E-20	0.050	332.0	7.65E-20	0.050	338.0	8.88E-20	0.050
342.0	8.88E-20	0.050	346.0	7.89E-20	0.050	349.0	7.89E-20	0.050	354.0	9.13E-20	0.050	355.0	8.14E-20	0.050
364.0	5.67E-20	0.050	368.0	6.66E-20	0.050	369.0	8.39E-20	0.050	370.0	8.39E-20	0.050	372.0	3.45E-20	0.050
374.0	3.21E-20	0.050	376.0	2.47E-20	0.050	377.0	2.47E-20	0.050	380.0	3.58E-20	0.050	382.0	9.90E-21	0.050
386.0	0.00E+00	0.050												
Photolysis File = ACROLEIN														
250.0	1.80E-21	1.000	252.0	2.05E-21	1.000	253.0	2.20E-21	1.000	254.0	2.32E-21	1.000	255.0	2.45E-21	1.000
256.0	2.56E-21	1.000	257.0	2.65E-21	1.000	258.0	2.74E-21	1.000	259.0	2.83E-21	1.000	260.0	2.98E-21	1.000
261.0	3.24E-21	1.000	262.0	3.47E-21	1.000	263.0	3.58E-21	1.000	264.0	3.93E-21	1.000	265.0	4.67E-21	1.000
266.0	5.10E-21	1.000	267.0	5.38E-21	1.000	268.0	5.73E-21	1.000	269.0	6.13E-21	1.000	270.0	6.64E-21	1.000
271.0	7.20E-21	1.000	272.0	7.77E-21	1.000	273.0	8.37E-21	1.000	274.0	8.94E-21	1.000	275.0	9.55E-21	1.000
276.0	1.04E-20	1.000	277.0	1.12E-20	1.000	278.0	1.19E-20	1.000	279.0	1.27E-20	1.000	280.0	1.27E-20	1.000
281.0	1.26E-20	1.000	282.0	1.26E-20	1.000	283.0	1.28E-20	1.000	284.0	1.33E-20	1.000	285.0	1.38E-20	1.000
286.0	1.44E-20	1.000	287.0	1.50E-20	1.000	288.0	1.57E-20	1.000	289.0	1.63E-20	1.000	290.0	1.71E-20	1.000
291.0	1.78E-20	1.000	292.0	1.86E-20	1.000	293.0	1.95E-20	1.000	294.0	2.05E-20	1.000	295.0	2.15E-20	1.000
296.0	2.26E-20	1.000	297.0	2.37E-20	1.000	298.0	2.48E-20	1.000	299.0	2.60E-20	1.000	300.0	2.73E-20	1.000
301.0	2.85E-20	1.000	302.0	2.99E-20	1.000	303.0	3.13E-20	1.000	304.0	3.27E-20	1.000	305.0	3.39E-20	1.000
306.0	3.51E-20	1.000	307.0	3.63E-20	1.000	308.0	3.77E-20	1.000	309.0	3.91E-20	1.000	310.0	4.07E-20	1.000
311.0	4.25E-20	1.000	312.0	4.39E-20	1.000	313.0	4.44E-20	1.000	314.0	4.50E-20	1.000	315.0	4.59E-20	1.000
316.0	4.75E-20	1.000	317.0	4.90E-20	1.000	318.0	5.05E-20	1.000	319.0	5.19E-20	1.000	320.0	5.31E-20	1.000
321.0	5.43E-20	1.000	322.0	5.52E-20	1.000	323.0	5.60E-20	1.000	324.0	5.67E-20	1.000	325.0	5.67E-20	1.000
326.0	5.62E-20	1.000	327.0	5.63E-20	1.000	328.0	5.71E-20	1.000	329.0	5.76E-20	1.000	330.0	5.80E-20	1.000
331.0	5.95E-20	1.000	332.0	6.23E-20	1.000	333.0	6.39E-20	1.000	334.0	6.38E-20	1.000	335.0	6.24E-20	1.000
336.0	6.01E-20	1.000	337.0	5.79E-20	1.000	338.0	5.63E-20	1.000	339.0	5.56E-20	1.000	340.0	5.52E-20	1.000
341.0	5.54E-20	1.000	342.0	5.53E-20	1.000	343.0	5.47E-20	1.000	344.0	5.41E-20	1.000	345.0	5.40E-20	1.000
346.0	5.48E-20	1.000	347.0	5.90E-20	1.000	348.0	6.08E-20	1.000	349.0	6.00E-20	1.000	350.0	5.53E-20	1.000
351.0	5.03E-20	1.000	352.0	4.50E-20	1.000	353.0	4.03E-20	1.000	354.0	3.75E-20	1.000	355.0	3.55E-20	1.000
356.0	3.45E-20	1.000	357.0	3.46E-20	1.000	358.0	3.49E-20	1.000	359.0	3.41E-20	1.000	360.0	3.23E-20	1.000
361.0	2.95E-20	1.000	362.0	2.81E-20	1.000	363.0	2.91E-20	1.000	364.0	3.25E-20	1.000	365.0	3.54E-20	1.000
366.0	3.30E-20	1.000	367.0	2.78E-20	1.000	368.0	2.15E-20	1.000	369.0	1.59E-20	1.000	370.0	1.19E-20	1.000
371.0	8.99E-21	1.000	372.0	7.22E-21	1.000	373.0	5.86E-21	1.000	374.0	4.69E-21	1.000	375.0	3.72E-21	1.000
376.0	3.57E-21	1.000	377.0	3.55E-21	1.000	378.0	2.83E-21	1.000	379.0	1.69E-21	1.000	380.0	8.29E-24	1.000
381.0	0.00E+00	1.000												